Atomistic modelling of phase transformation at large time and length scales: atomistic phase field approach

Helena Zapolsky,

University of Rouen Normandie, GPM, UMR 6634, Saint-Etienne du Rouvray, France

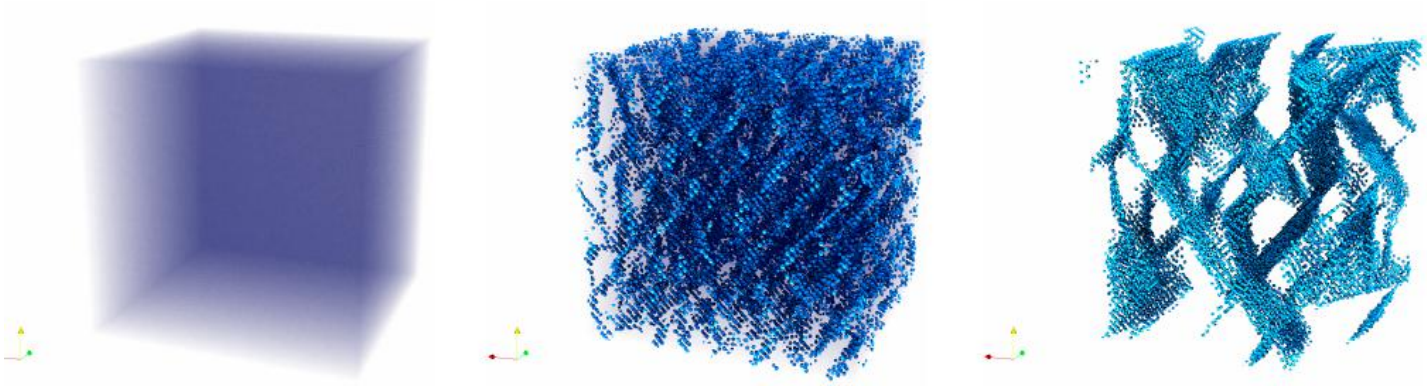

March 20th, 2023 Workshop II: Scale-Bridging MaterialsModeling at Extreme Computational Scales

Acknowledgements




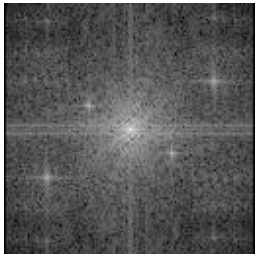


G. Demange , M. Lavrskyi, *O. Nakonechna,* ***Y. Borges Gomes Lima,***
A. Vaugeois, ***R. Patte***
GPM University of Rouen, France

A.G. Khachaturyan
Rutgers University, Piscataway, NJ

Microstructure of alloys

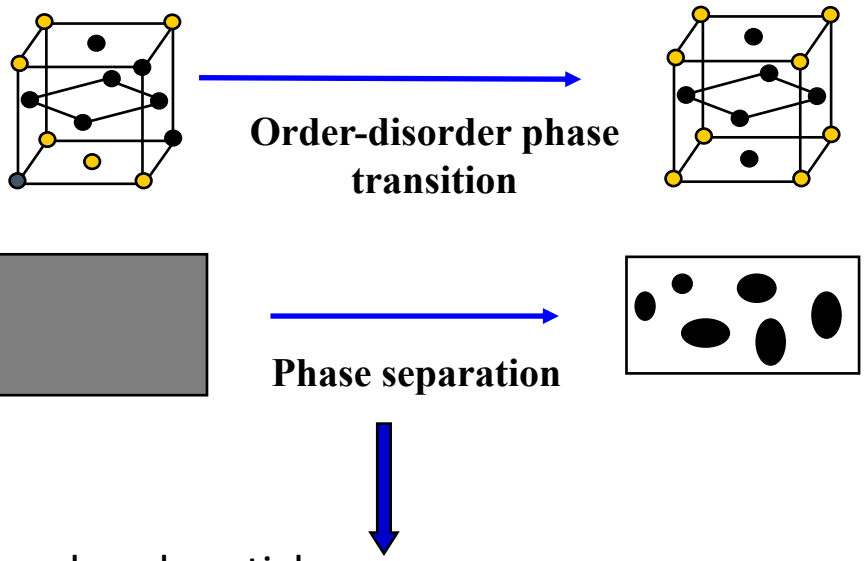

Ni-8%Al-6%Ti aged at 800°C during 45h

Phase Field modelling

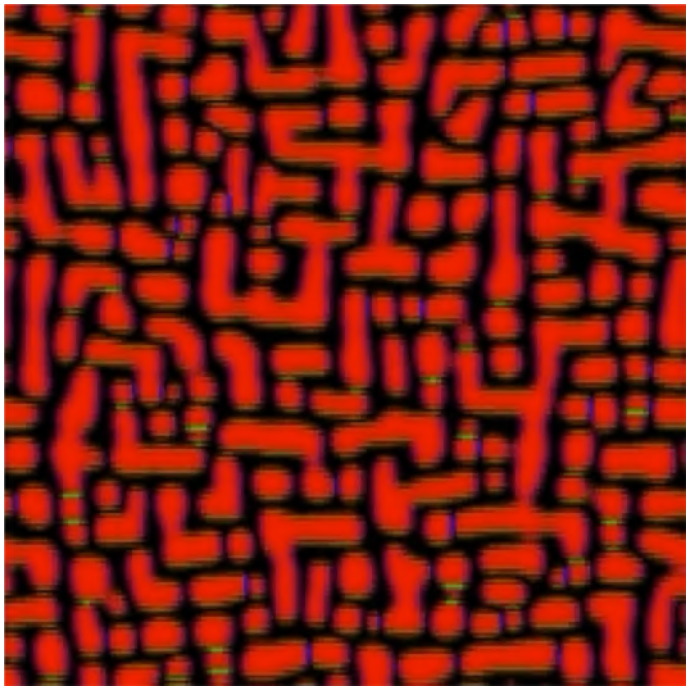

J Boisse et al Acta Mat. 55, 2007

Displacive transformations

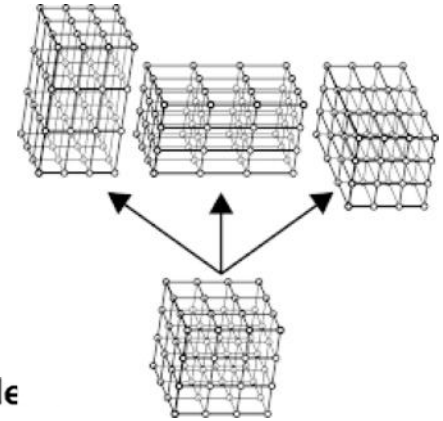

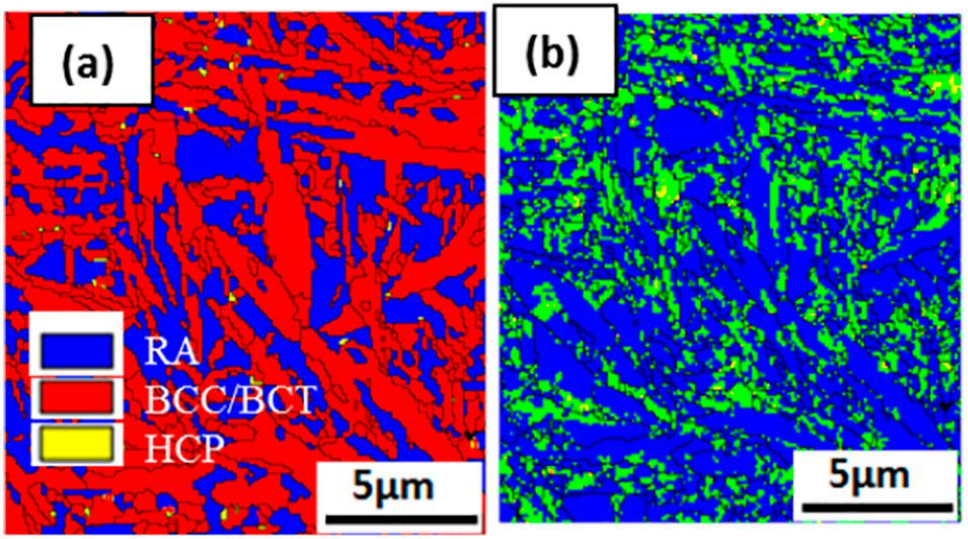

Microstructures of the steel

R. Hossain et al Mat. Charact. 149, 2019

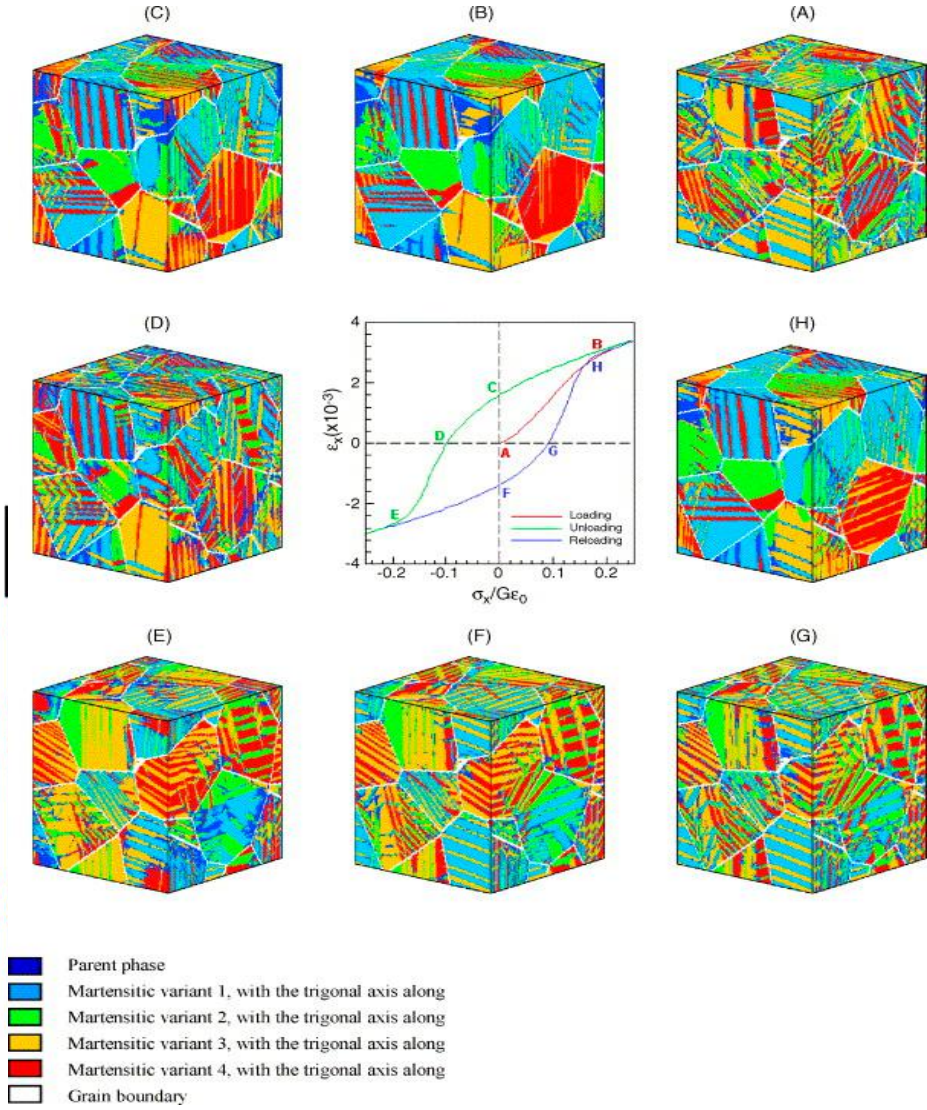

cubic → trigonal martensitic transformation in a polycrystalline system

Y.M. Jin et al Acta Mater., 49 (2001)

Grain boundary segregation induced strengthening of an ultrafine-grained austenitic stainless steel

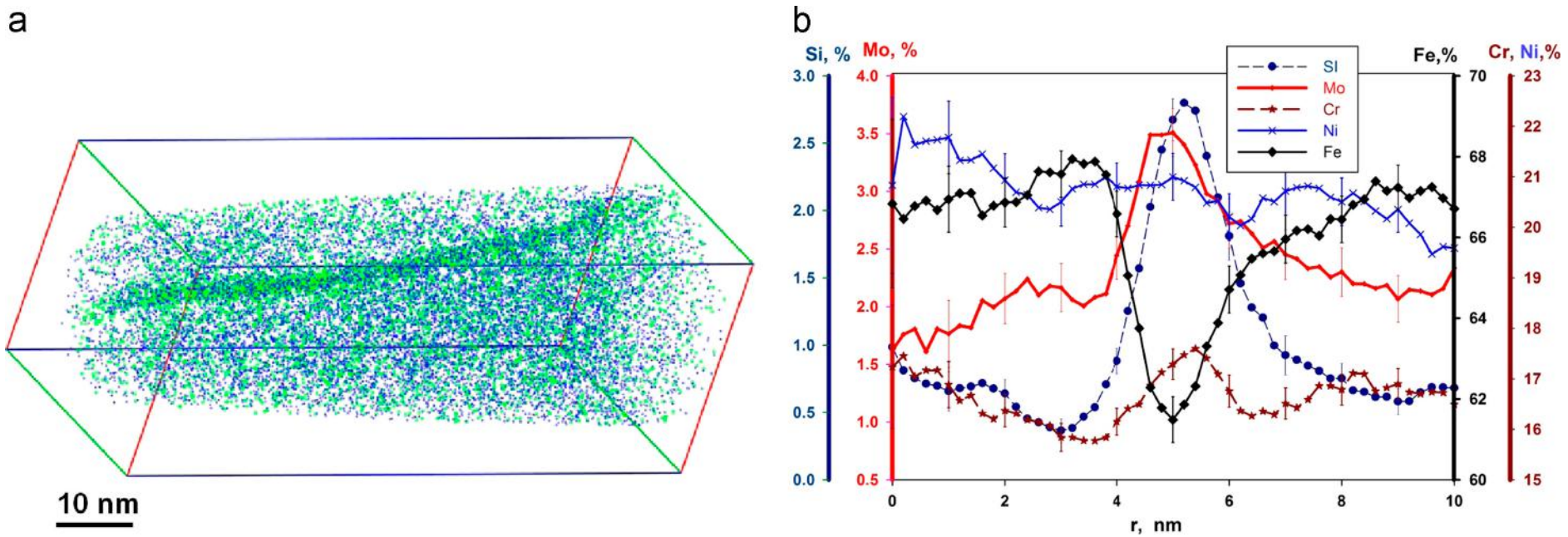

An APT analysis of HPT 400 °C 316 steel reveals formation of Mo–Cr–Si rich segregation at a grain boundary—Mo and Si atoms are displayed.

M.M. Abramova et al, Materials Letters, 136, 2014

Landau Khalatnikov kinetic equation (1954)

Landau-Khalatnikov relaxation equation

$$\frac{d\psi(\vec{r},t)}{dt} = -\gamma \frac{\partial F}{\partial \psi(\vec{r},t)}$$

Atomistic description (nm)

Continuos field description (µm)

Microscopique kinetic equation
Atomic density function theory

$$\frac{dP(\vec{r},t)}{dt} = \sum_{\vec{r}'} L(\vec{r}-\vec{r}') \frac{\partial F}{\partial P(\vec{r}',t)}$$

Time dependent Ginzburg-Landau equation

$$\frac{\partial \eta(\vec{r},t)}{\partial t} = -L\left(\frac{\delta F}{\delta \eta(\vec{r},t)}\right) + \zeta_\eta(\vec{r},t)$$

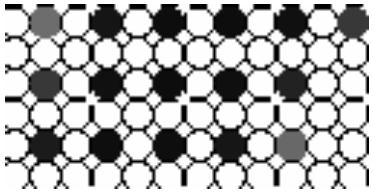

?

Cahn-Hilliard equation for concentrations

$$\frac{\partial c(\vec{r},t)}{\partial t} = \vec{\nabla} M \vec{\nabla}\left(\left(\frac{\delta F}{\delta c(\vec{r},t)}\right)\right) + \varsigma_c(\vec{r},t)$$

P(r) is the probability to find atom in position r.

Phase field variables:
Concentration c(r)
Ordre parametre η(r)

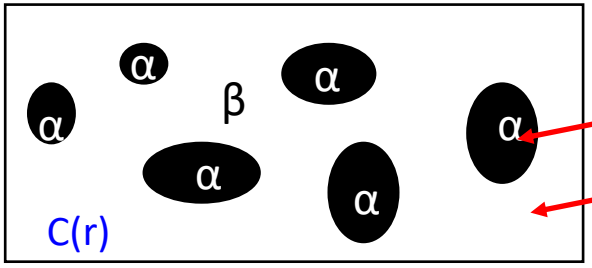

Addressable Scales

Spatial scales: Atomic scale Nano-scale Micron and sub-micron scale

Time scale: sub-second - up to years

Phenomenological approches

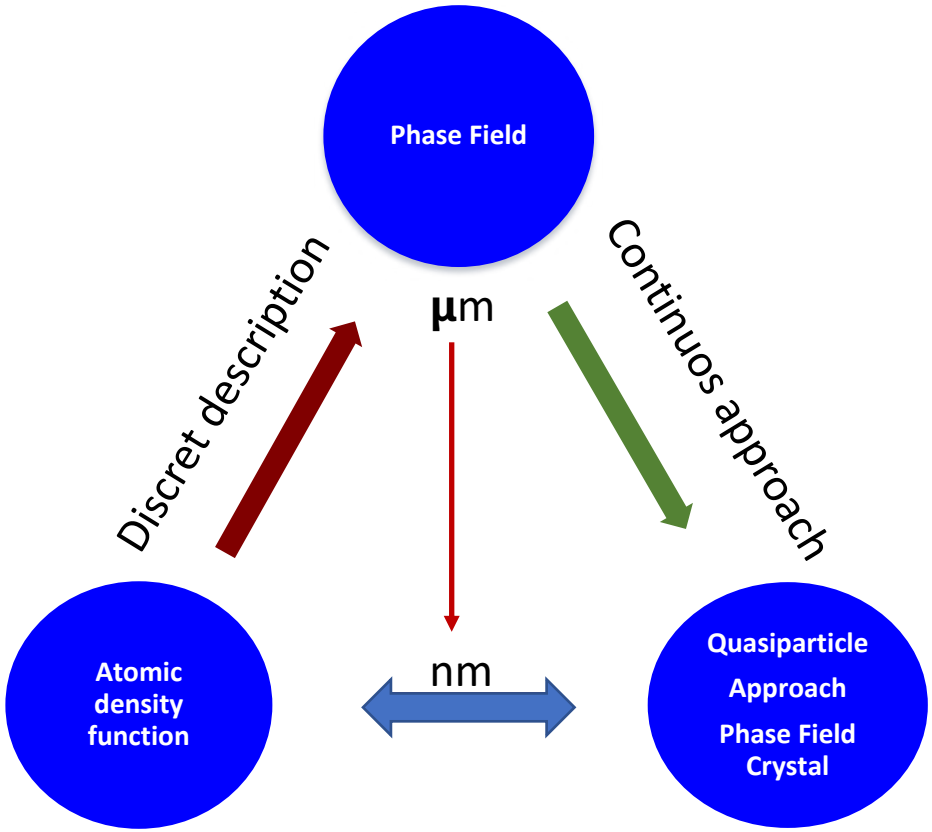

Stability of the system with respect to infinitesimal fluctuations

$$\delta c(r) = c(r) - \bar{c}$$

Free energy of heterogeneous system in continuous approximation

$$F = \int_V \left[(f(c) + \frac{1}{2}\beta(c)(\nabla c)^2) dV \right]$$

Variation of free energy with respect to small fluctuations

$$\delta c(r) = c(r) - \bar{c} = \frac{1}{N}\sum_k c(k) e^{ikr}$$

FT

$$\Delta F = \frac{1}{2}\int b(k)\left|c(k)\right|^2 \frac{d^3k}{(2\pi)^3}$$

min F ⟹ **min b(k)**

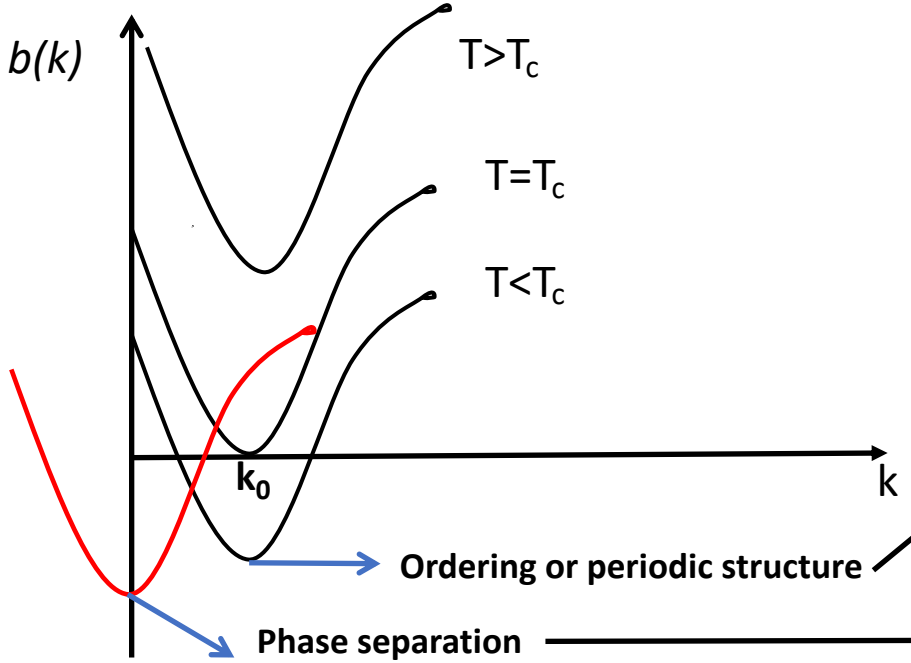

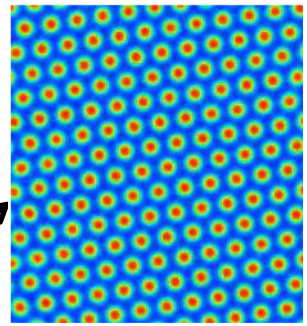

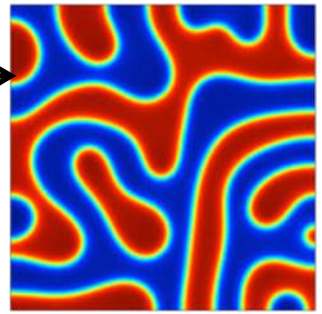

Two types of minima:

$$\left.\frac{\partial b(k)}{\partial k}\right|_{k=k_j} = 0$$

k=0 separation

k≠0 periodic structures

Brazovskii model of crystalisation

The addition Ψ^3 in the free energy functional break ± symmetry (Brazovskii energy, 1975)

$$F = \int d\mathbf{r}\left[\frac{1}{2}\psi(-\varepsilon + (k_0^2 + \nabla^2)^2)\psi + \alpha\frac{\psi^3}{3} + \frac{\psi^4}{4}\right]$$

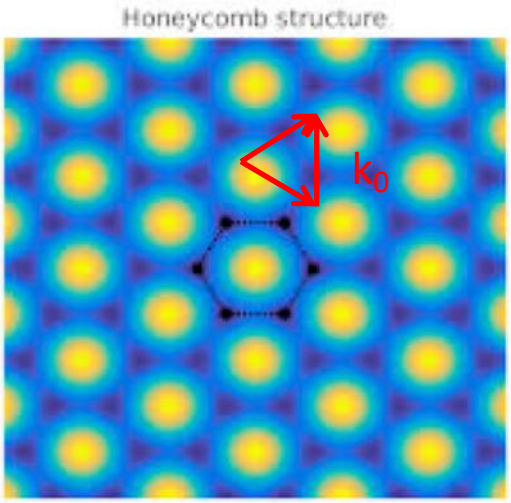

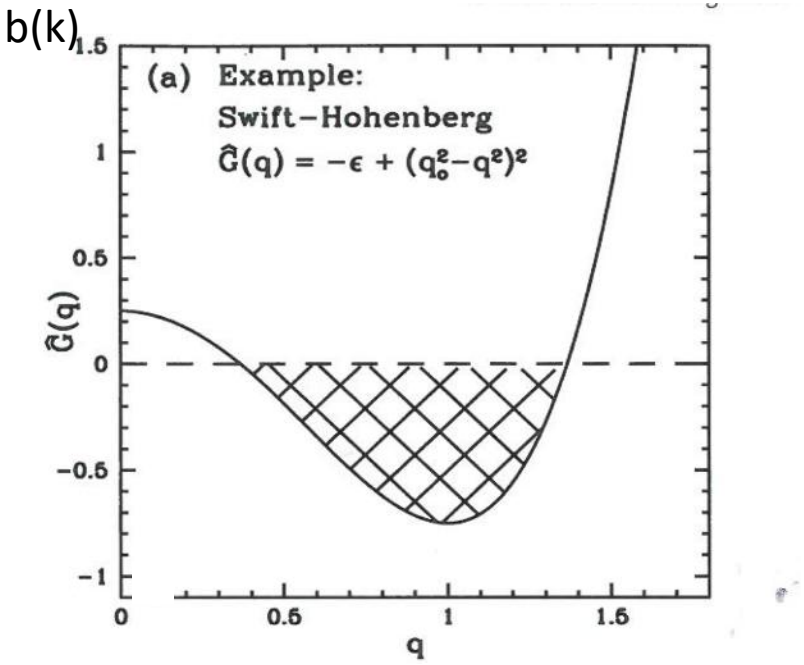

for ε=3/4 and k_0=1

$$\frac{\partial \psi}{\partial t} = -L\frac{\delta F}{\delta \psi} = L(\varepsilon - (q_0^2 + \nabla^2)^2 \psi - \alpha \psi^2 - \psi^3)$$

Swift-Hohenberg model of convection

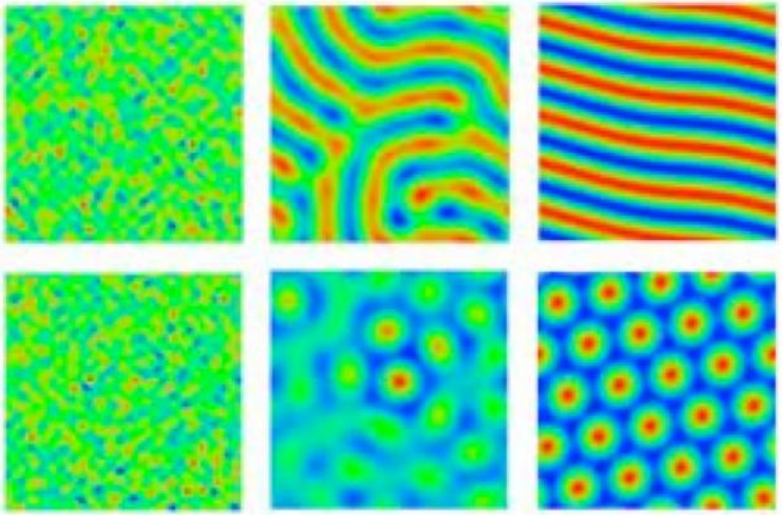

stripes

honeycomb structure.

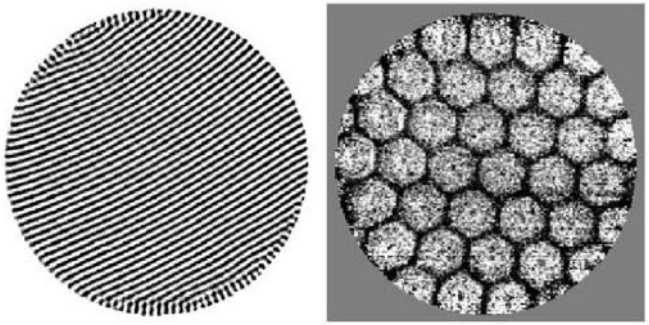

Rayleigh–Bénard convection

Phase Field Crystal method (K. Elder, 2002) -> zones with high concentration-> atoms

Limit transition to the Landau theory

$$F = \int \frac{1}{2} \sum_{\alpha\beta} V_{\alpha\beta}(k)\Phi_{\alpha}(k)\Phi^{*}_{\beta}(k)\frac{d^3k}{(2\pi)^3} + \int_V f(\{\rho_{\alpha}(r)\})d^3r \qquad (1)$$

Where $V_{\alpha\beta}(\mathbf{k})$ is the Fourier transforms of the effective potentials $W_{\alpha\beta}(\mathbf{r})$:

$$\mathrm{V}(\boldsymbol{k}) = \int_{\mathrm{V}} \mathrm{W}(\boldsymbol{r})\, exp(-\mathrm{i}\boldsymbol{k}\boldsymbol{r})\mathrm{d}^3\mathrm{r}$$

Using Taylor expansion of $V_{\alpha\beta}(\mathbf{k})$ in k

$$V_{\alpha\beta}(k) = A_0^{\alpha\beta} + \frac{1}{2!}A_2^{\alpha\beta}k^2 + \frac{1}{4!}A_4^{\alpha\beta}k^4 + \ldots + \frac{1}{n!}A_n^{\alpha\beta}$$

Eq.(1) is a generalized **Landau gradient expression**:

$$F = \int_V \sum_{\alpha\beta}\left(\frac{1}{2!}A_o^{\alpha\beta}\rho_{\alpha}(\mathbf{r})\rho_{\beta}(\mathbf{r}) + \frac{1}{2!}A_2^{\alpha\beta}\nabla\rho_{\alpha}(\mathbf{r})\nabla\rho_{\beta}(\mathbf{r}) + \frac{1}{4!}A_4^{\alpha\beta}\nabla^2\rho_{\alpha}(\mathbf{r})\nabla^2\rho_{\beta}(\mathbf{r}) + \ldots\right)d^3r$$
$$+ \int_V f(\{\rho(\mathbf{r})_{\alpha}\})d^3r$$

The **Phase Field Crystal model** has used two first terms of the gradient expansion of the Landau theory.

From Atomic density function theory on constrained lattice to continuous approach

$$F = F_{chem} + E_{elast}$$

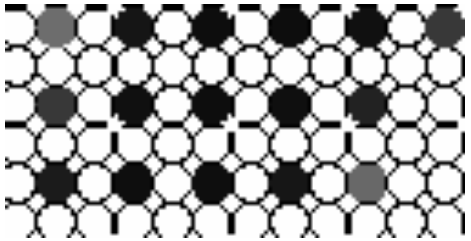

$$F_{chem} = \frac{1}{2}\sum_{r,r'} V(r-r')p(r)p(r') + k_B T \sum_{\vec{r}} \left\{ p(r)Ln(p(r) + \left[1-p(r)\right]Ln\left[1-(p(r)\right]\right\}$$

$$E_{elast} = \frac{1}{2}\sum_{pq} \int \frac{d^3k}{(2\pi)^3} B_{pq}(\mathbf{n})\theta_p(\mathbf{k})\theta_q^*(\mathbf{k})$$

Microscopic kinetic Onsager equation

$$\frac{dP(r,t)}{dt} = \frac{1}{k_B T}\sum_{\alpha,\beta}\sum_{r'} L_{\alpha\beta}(r-r')c_\alpha c_\beta \frac{\partial F}{\partial P(r',t)}$$

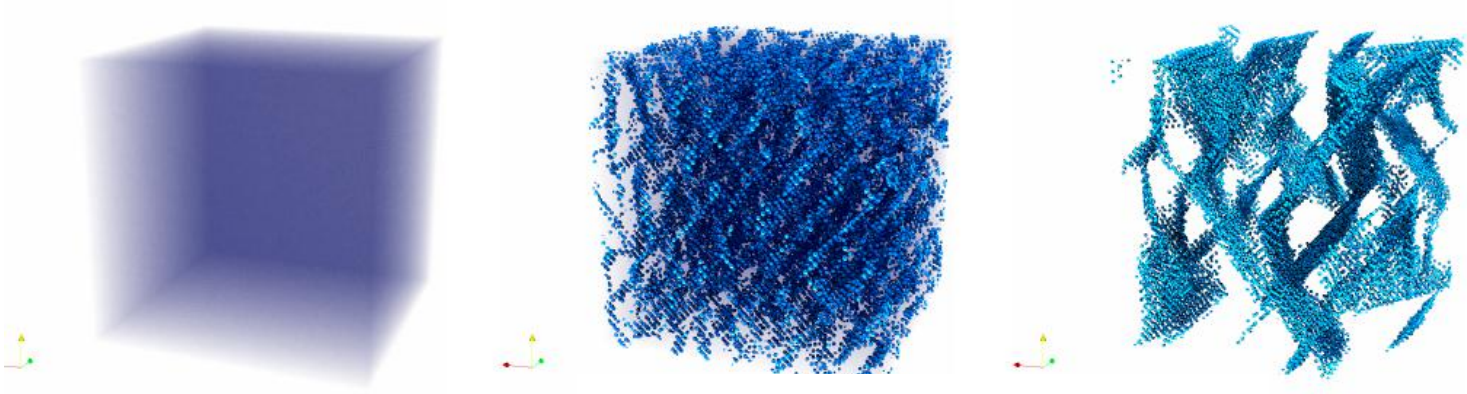

Carbide formation in Fe-C system

F. Scwab et al. submitted to Acta Mat.

Carbon atoms in the bcc lattice

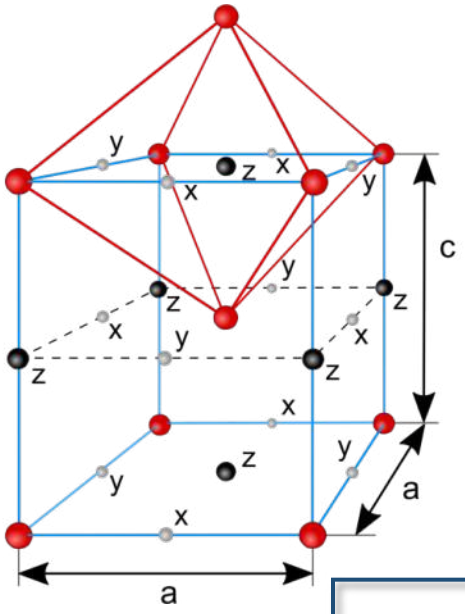

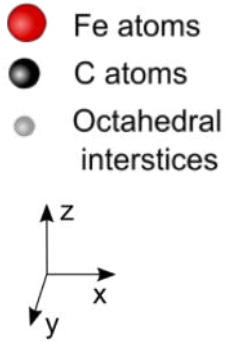

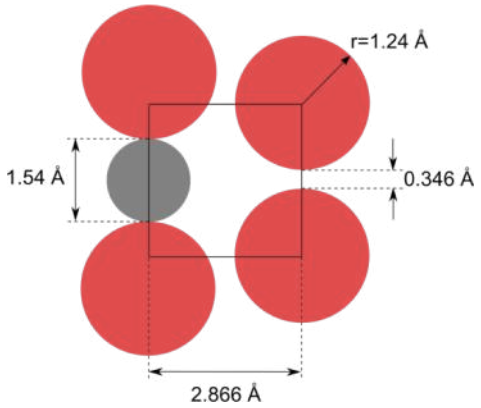

Deformation matrix

$$u_{ij}(1)=\begin{pmatrix} u_{33} & 0 & 0 \\ 0 & u_{11} & 0 \\ 0 & 0 & u_{11} \end{pmatrix}$$

$$u_{ij}(2)=\begin{pmatrix} u_{11} & 0 & 0 \\ 0 & u_{33} & 0 \\ 0 & 0 & u_{11} \end{pmatrix}$$

$$u_{ij}(3)=\begin{pmatrix} u_{11} & 0 & 0 \\ 0 & u_{11} & 0 \\ 0 & 0 & u_{33} \end{pmatrix}$$

Concentration expansion coefficients

$$u_{11}=\frac{a-a_0}{a_0\bar{c}_c};\qquad u_{33}=\frac{c-a_0}{a_0\bar{c}_C}$$

Interaction potential consists of elastic and chemical parts:

$$\tilde{w}_{pq}(\mathbf{k})=\tilde{w}^{elas}_{pq}(\mathbf{k})+\tilde{w}^{chem}_{pq}(\mathbf{k})$$

$$p,q=1,2,3$$

Elastic part of the interaction potential:

$$\tilde{w}_{pq}^{elast}(\mathbf{k}) = -F_i^{oct}(p,\mathbf{k}) G_{ij}(\mathbf{k}) F_i^{*oct}(q,\mathbf{k})$$

Kanzaki forces

$$F_x^{oct}(3,\mathbf{k}) = -ia_0^2\sigma_{11}^0 \sin\left(\frac{k_x a_0}{2}\right)\cos\left(\frac{k_y a_0}{2}\right)$$

$$F_y^{oct}(3,\mathbf{k}) = -ia_0^2\sigma_{11}^0 \cos\left(\frac{k_x a_0}{2}\right)\sin\left(\frac{k_y a_0}{2}\right)$$

$$F_z^{oct}(3,\mathbf{k}) = -ia_0^2\sigma_{33}^0 \sin\left(\frac{k_z a_0}{2}\right)$$

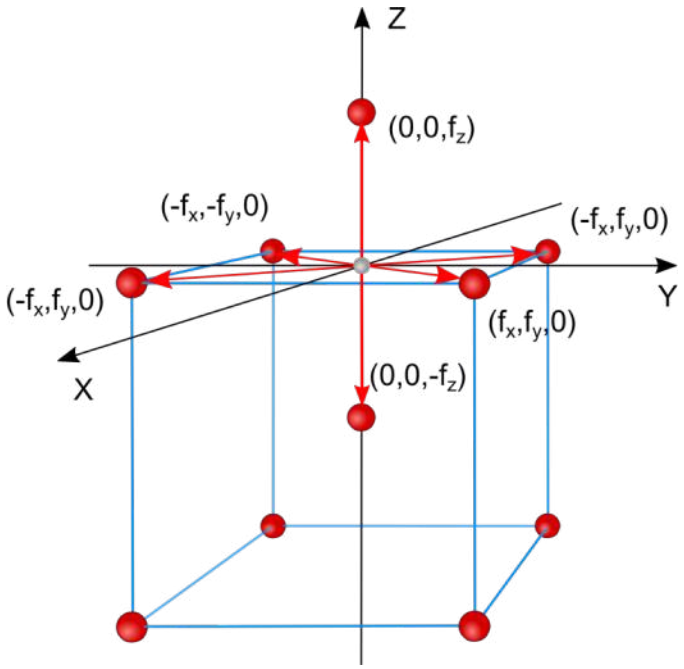

$$\sigma_{11}^0 = (C_{11} + C_{12})\, u_{11} + C_{12} u_{33}$$
$$\sigma_{33}^0 = C_{11} u_{33} + 2C_{12} u_{11}$$

Green function

$$G_{ij}(\mathbf{k}) = \left[D_{ij}(\mathbf{k})\right]^{-1}$$

CHEMICAL PART OF INTERACTION POTENTIAL

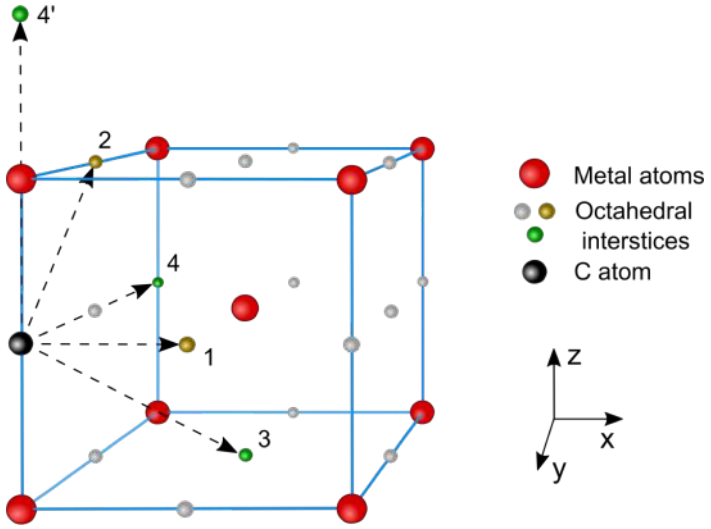

$$W_1^{chem} = 3.13$$
$$W_2^{chem} = 0.87$$
$$W_3^{chem} = 0.27$$
$$W_4^{chem} = 1.4$$
$$W_4^{chem^*} = 0.23$$

$$\tilde{w}_{11}^{chem}(\mathbf{k}) = 8W_3 \cos\left(\frac{k_x a_0}{2}\right)\cos\left(\frac{k_y a_0}{2}\right)\cos\left(\frac{k_z a_0}{2}\right) + 2W_4\left(\cos(k_y a_0) + \cos(k_z a_0)\right) + 2W_4^{*}\cos(k_x a_0)$$

$$\tilde{w}_{12}^{chem}(\mathbf{k}) = 2W_1 \cos\left(\frac{k_z a_0}{2}\right) + 4W_2 \cos\left(\frac{k_y a_0}{2}\right)\cos\left(\frac{k_x a_0}{2}\right)$$

A. Udyansky, J. von Pezold, A. Dick, and J. Neugebauer. Phys. Rev. B, 83:184112, 2011

Interaction potential

$$\tilde{w}_{pq}(\mathbf{k}) = -\frac{F_i^{oct}(p,\mathbf{k}) G_{ij}(\mathbf{k}) F_i^{*oct}(q,\mathbf{k})}{a_0^3 C_{44} u_{33}^2} + W_0 \frac{\tilde{w}_{pq}^{chem}(\mathbf{k})}{a_0^3 C_{44} u_{33}^2}$$

Dimensionless parameter

$a_0^3 C_{44} u_{33}^2 = 12.17$ eV

Concentration expansion coefficients [1]

$u_{11} = -0.09$

$u_{33} = 0.86$

$t_1 = u_{11}/u_{33} = -0.1$

Fe_α

$a_0 = 2{,}865$ Å

$C_{11} = 242$ GPa

$C_{12} = 146.5$ GPa

$C_{44} = 112$ GPa

Carbon diffusion in martensite phase at room temperature

T=40° C

ρ_c=0.4w%

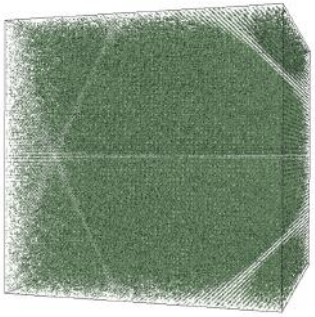

t = 0

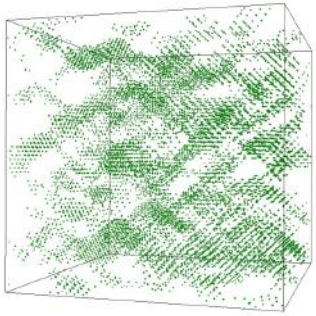

t =280000

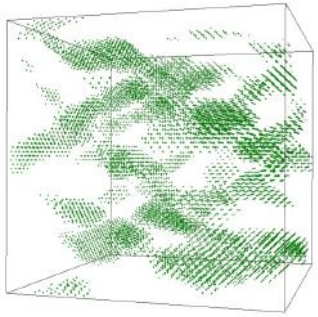

t = 600000

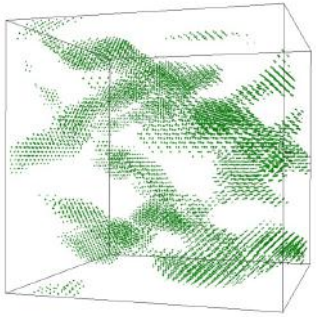

t = 8000000

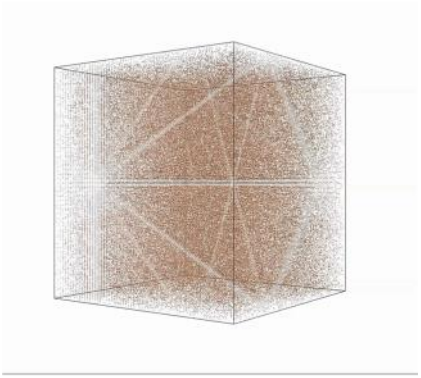

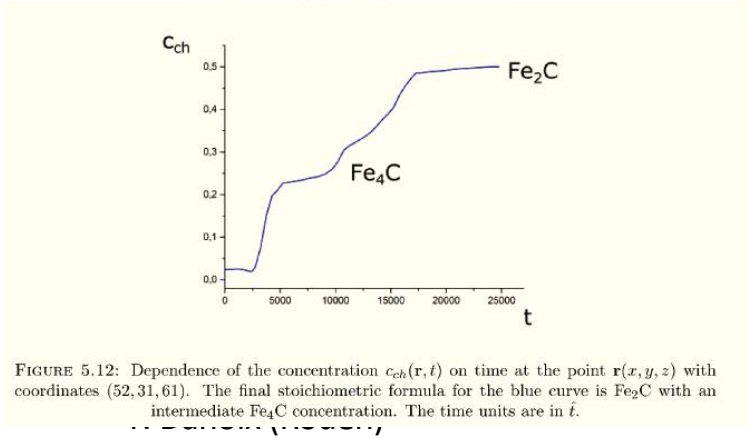

FIGURE 5.12: Dependence of the concentration $c_{ch}(\mathbf{r}, t)$ on time at the point $\mathbf{r}(x, y, z)$ with coordinates $(52, 31, 61)$. The final stoichiometric formula for the blue curve is Fe_2C with an intermediate Fe_4C concentration. The time units are in $\hat{t}$.

Diffraction of carbon reach zones observed after aging at room temperature

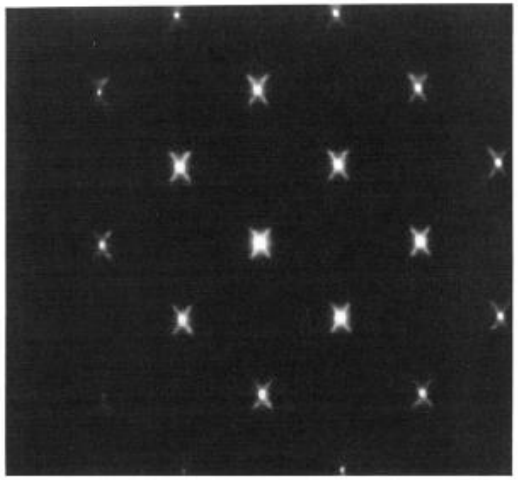

diffraction pattren obtained from Fe-15Ni-1C marteniste after aging at room temperature for 26 min (K.A. Taylor et all. Met.Trans.A V.20A, 1989)

Diffraction pattern from simulation

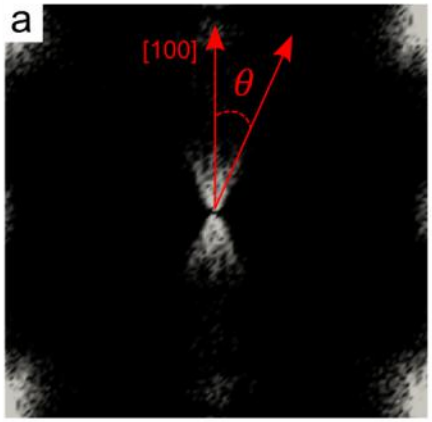

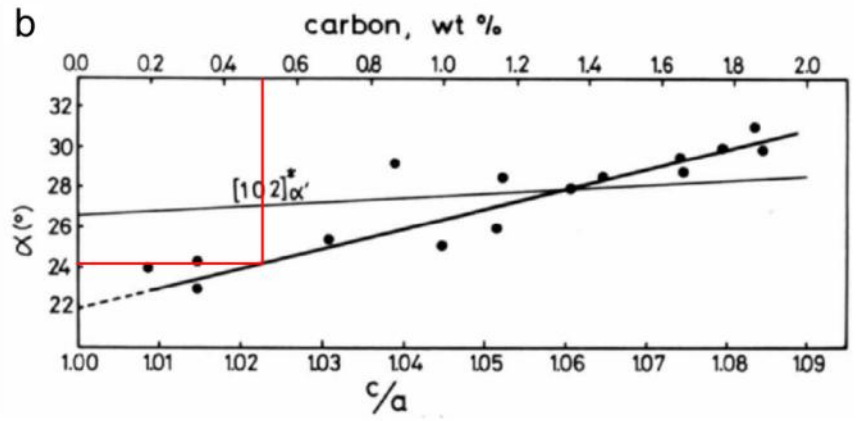

$\overline{c}_C = 0.51\ \text{wt.\%}$

$\theta_{obtained} \approx 23.4° \Rightarrow \sim[2\bar{1}0]$

$\theta_{exp} \approx 24°$

M. Kusunoki and S. Nagakura, *J. Appl. Cryst*, **14** (1981)

η-Fe_2C carbide

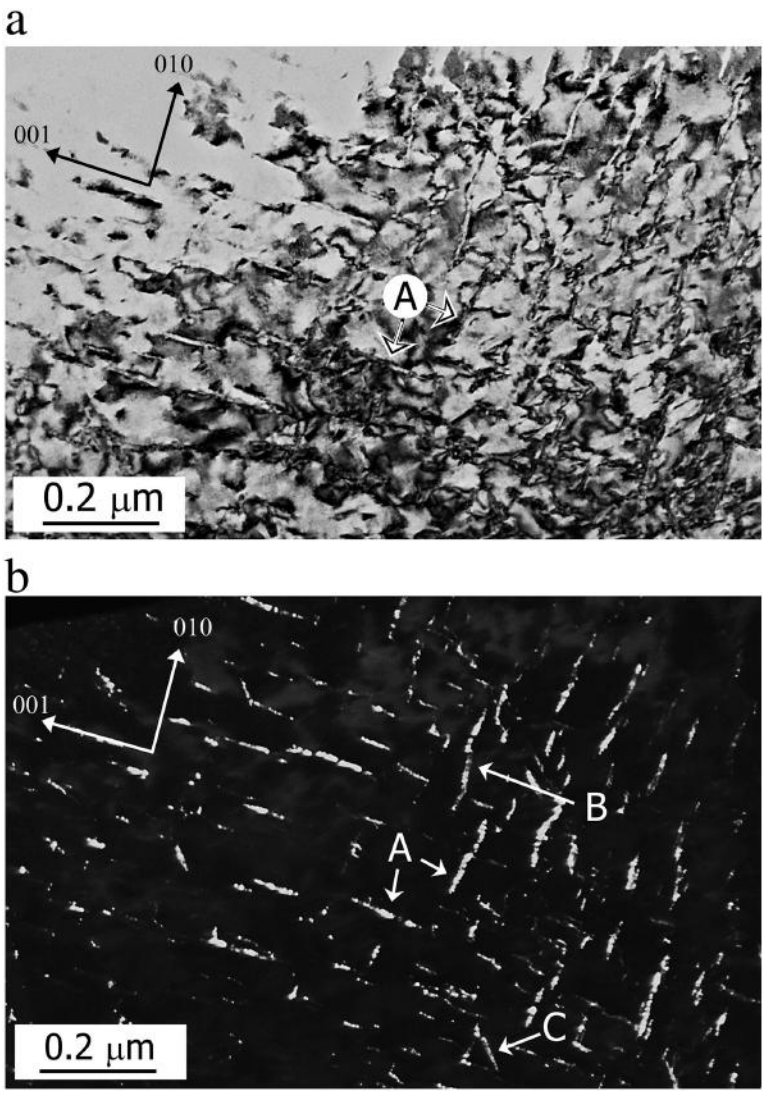

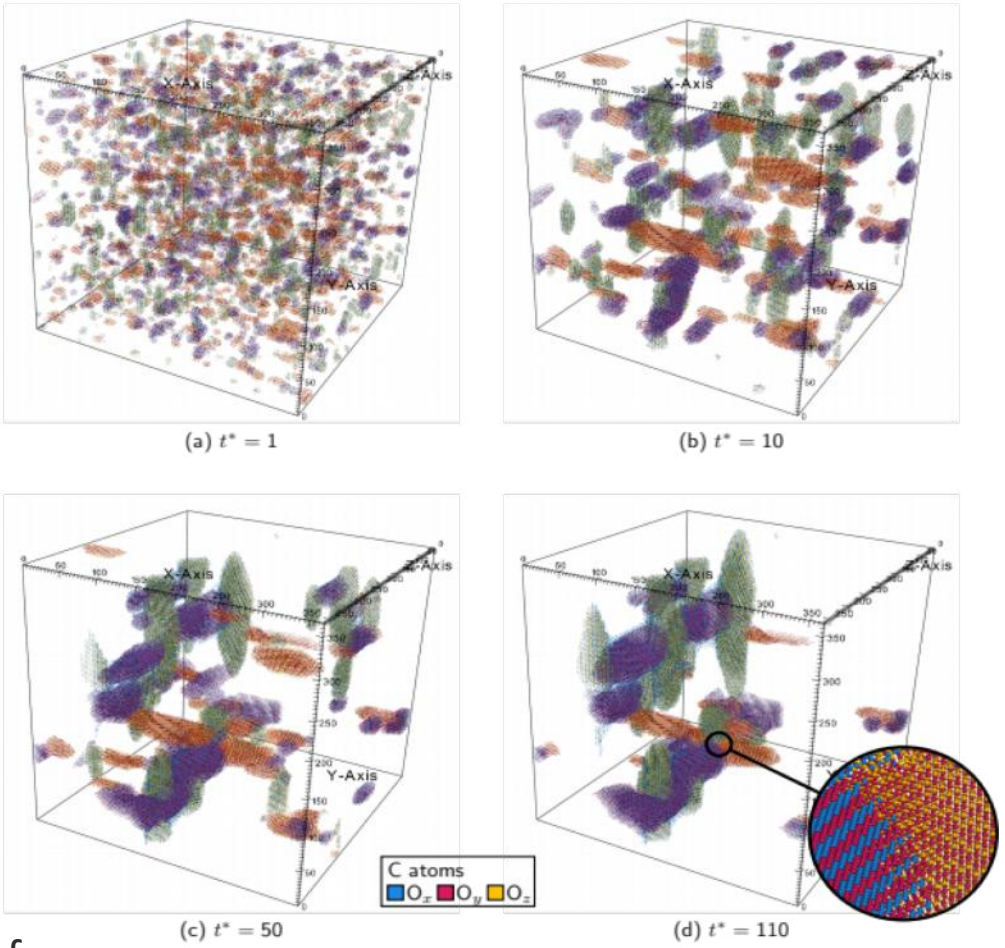

Transition-iron-carbide precipitates in a lath of tempered martensite. (a) Bright-field and (b) centered-dark-field TEM images.

S.W.Thompson Mater. Charact. V.106, 2015

Schwab et al npj Comput Mat under revision

From discrete to continuum ADF model

Rigide Ising lattice

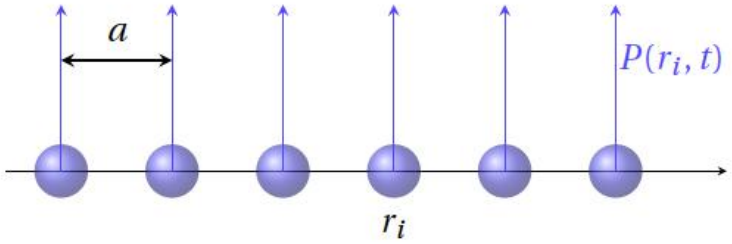

(a) Probability $P(r_i, t)$ to find atom on site r_i

- $\mathbb{P}(r)$: probability to find atom at position r
- 1 atome $\Leftrightarrow$ 1 site

$$\sum_r \mathbb{P}(r) = N_{atoms}$$

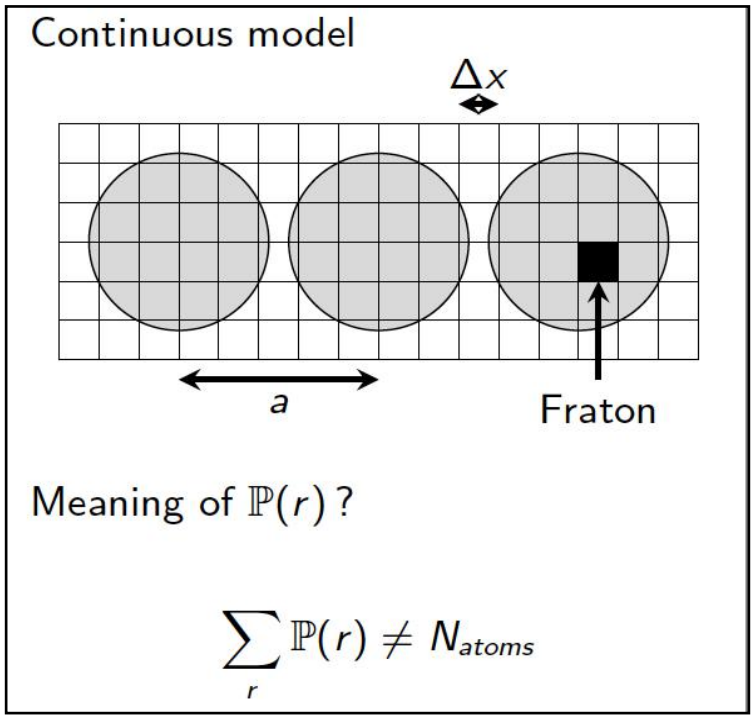

(M. Lavrskiy et al.,npj computational materials 2017)

$$\sum_r \mathrm{P}(\mathbf{r}) = N_{fraton}$$

The Fourier Transform representation of the model Hamiltonian:

$$H = \frac{1}{2N} \sum_{\boldsymbol{k}} \sum_{\alpha=1}^{\alpha=m} \sum_{\beta=1}^{\beta=m} \tilde{w}_{\alpha\beta}(\boldsymbol{k})\, \tilde{\rho}_{\alpha}(\boldsymbol{k}) \tilde{\rho}_{\beta}(\boldsymbol{k})^{*}$$

Model Potential $$W_{\alpha\beta}(\boldsymbol{r}-\boldsymbol{r}') = \underbrace{\theta_{\alpha}(\boldsymbol{r}-\boldsymbol{r}')\delta_{\alpha\beta}}_{\text{Short range}} + \underbrace{\lambda_{\alpha\beta} W^{\mathrm{LR}}_{\alpha\beta}(\boldsymbol{r}-\boldsymbol{r}')}_{\text{Long range}}.$$

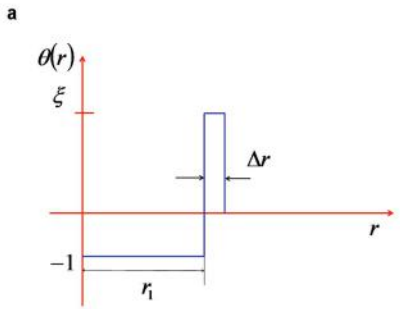

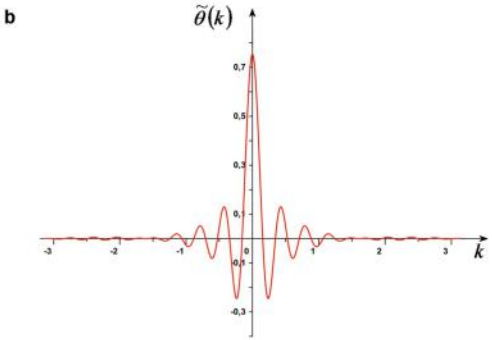

$$\theta_{\alpha}(\boldsymbol{r}) = \begin{cases} -1 & \text{if} \quad r \le R_{\alpha} \\ \xi & \text{if} \quad R_{\alpha} < r \le R_{\alpha} + \Delta R_{\alpha} \\ 0 & \text{otherwise.} \end{cases}$$

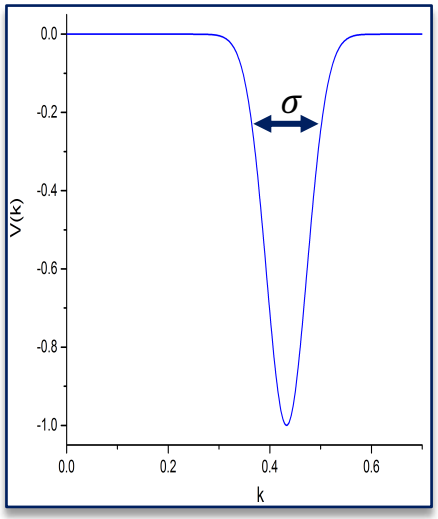

Exemple bcc structure

$$\hat{W}^{\mathrm{LR}}(k) = -\exp\left(-\frac{(k-k^{\mathrm{bcc}})^2}{2(\sigma^{\mathrm{bcc}})^2}\right)$$

Principal loading conditions – calculation of elastic constants

1) hydrostatic, $(x, y, z) \rightarrow (1-\varepsilon)x, (1-\varepsilon)y, (1-\varepsilon)z,$
2) orthorhombic, $(x, y, z) \rightarrow (1+\varepsilon)x, (1-\varepsilon)y, z$
3) monoclinique $(x, y, z) \rightarrow x + \varepsilon y, y, z$

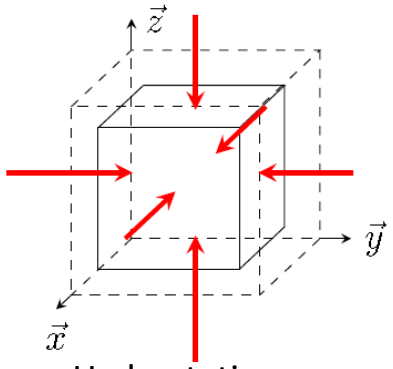

Hydrostatic

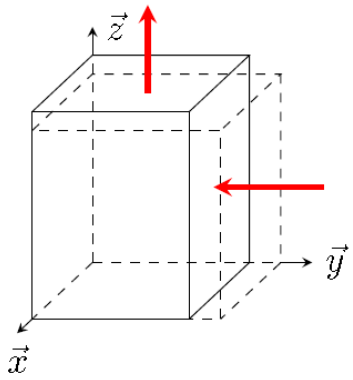

Orthorhombic

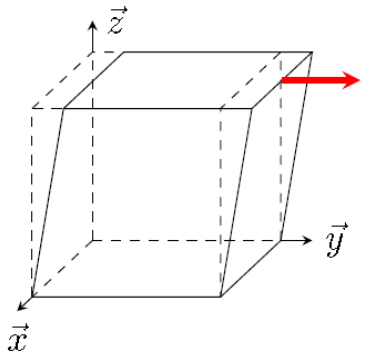

Monocline

$$F_{cubic.}(\varepsilon) = F_0 + V_0 \frac{3}{2}\left(C_{11} + 2C_{12}\right)\varepsilon^2$$

$$F_{orthor.}(\varepsilon) = F_0 + V_0\left(C_{11} - C_{12}\right)\varepsilon^2$$

$$F_{monoc.}(\varepsilon) = F_0 + V\frac{C_{44}}{2}\varepsilon^2$$

Kinetic equation (n-components alloy)

$$\frac{d\ \rho_\alpha(\mathbf{r},t)}{dt} = \sum_{\mathbf{r}'} L_{\alpha\beta}(\mathbf{r},\mathbf{r}')\ \frac{\delta F}{\delta \rho_\beta(\mathbf{r}',t)}$$

Free energy functional is:

$$F_{chem} = \frac{1}{2}\sum_{\alpha,\beta}\ \sum_{r,r'} V_{\alpha\beta}(r-r')p_\alpha(r)p_\beta(r') + k_B T \sum_{\alpha}\ \sum_{\vec{r}} \left\{ p_\alpha(r) Ln\left[p_\alpha(r)\right] + \left[1-p_\alpha(r)\ \right] Ln\left[1-(p_\alpha(r)\right] \right\}$$

Reduced variables:

time is measured in units of typical atomic migration time, τ_o

energy is measured in units of $k_B T_o$, where T_o is the solidification temperature

the grid lattice increment, l, (the spacing of the underlying Ising lattice), is defined as a fraction of the atomic radius

The numerical solution -> the semi-implicit Fourier spectral method

Self-assembly of fratons with only short range interaction

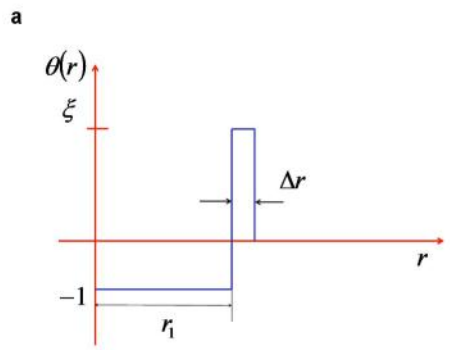

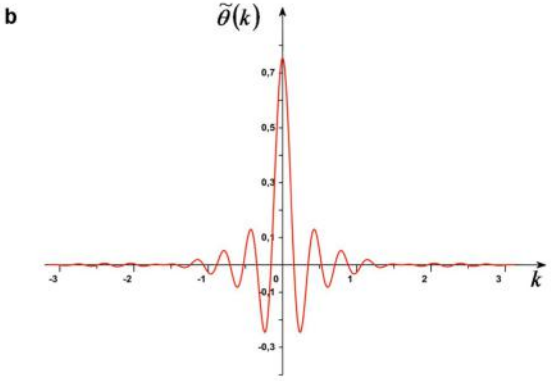

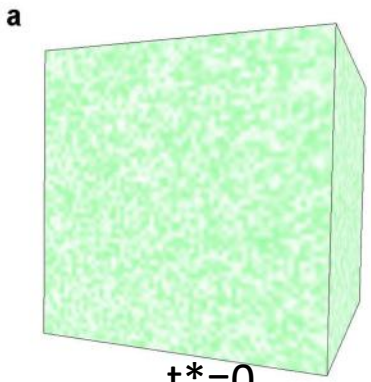

t*=0

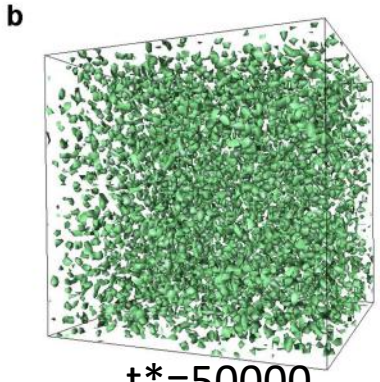

t*=50000

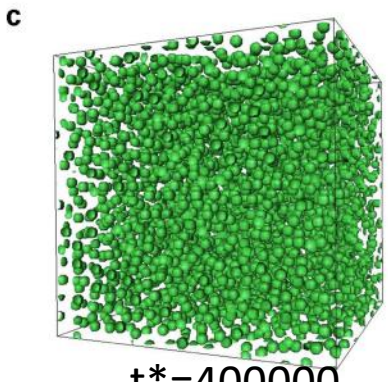

t*=400000

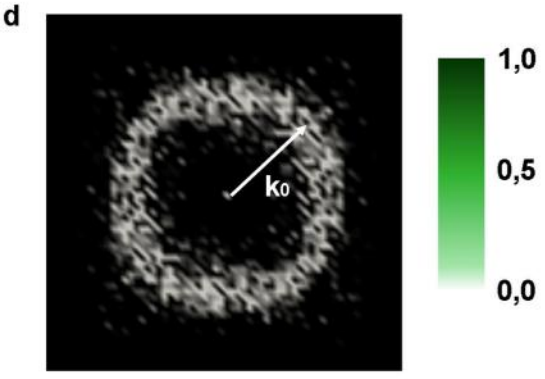

$\hat{\bar{\rho}} = 0.1$, $\hat{l} = 0.5$, $\Delta\hat{r} = 0.17$, and $\hat{T} = 0.63$ $\quad \hat{\lambda}_1 = 45.23$, $\xi = 4$

α-Fe polycrystal

- Short range potential :

$$V^{sr}(r) = \begin{cases} -1 & \text{if} \quad r < R \\ \xi & \text{if} \quad R \leq r \leq R + \Delta R \\ 0 & \text{if} \quad r > R + \Delta R \end{cases}$$

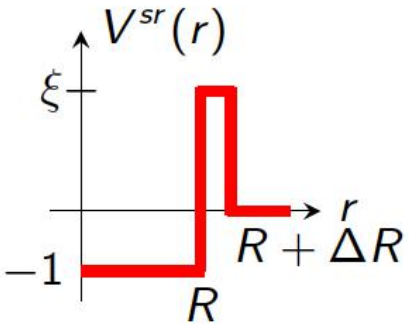

- Long range potential[1] :

$$V^{lr}(k) = 1 - \frac{k^4}{(k^2 - k_1^2)^2 + k_2^4}$$

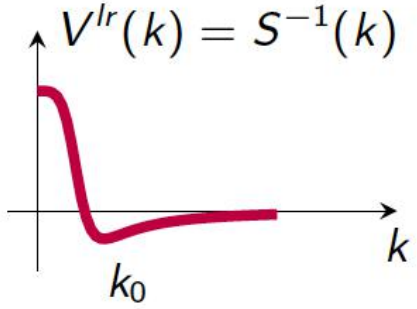

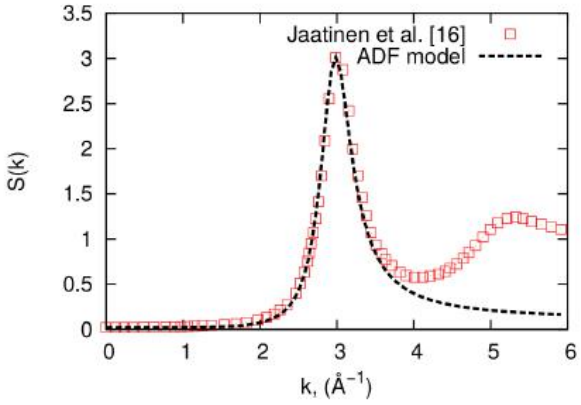

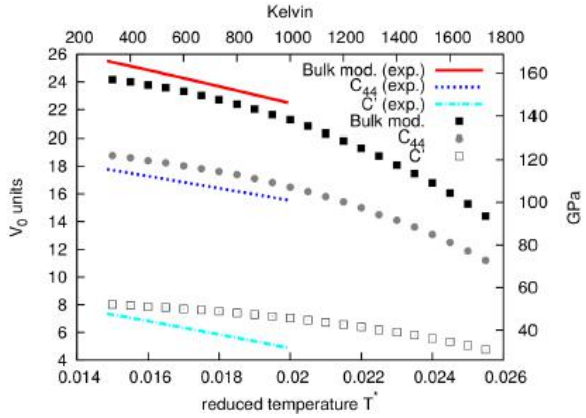

[1] O. Kapikranian, H. Zapolsky & al. Phys. Rev. B 00, 004100 (2015)

[16] Jaatinen et al. Phys. Rev. E 80 (2009) 031602

GB growth (tilt angle θ = 3.58°)

Dislocations
at GB

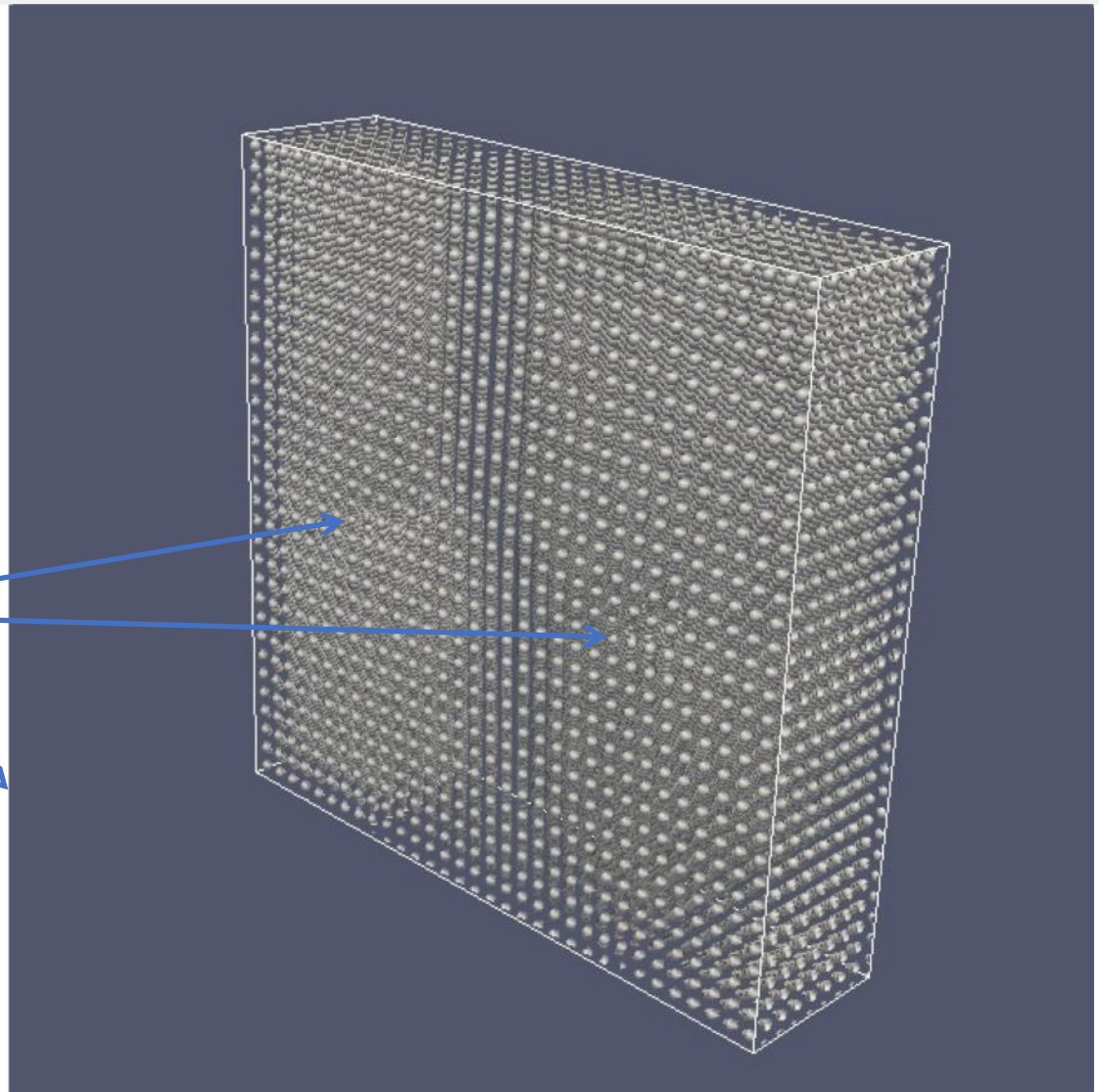

The atomic density function (ADF) model of tilt grain boundaries in α-Fe

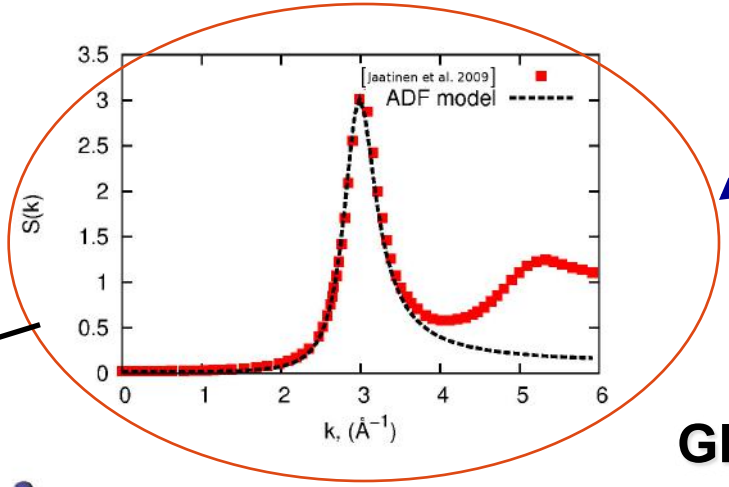

$V_{LR}(k)$

$T=0.9T_m$

Atomic configurations

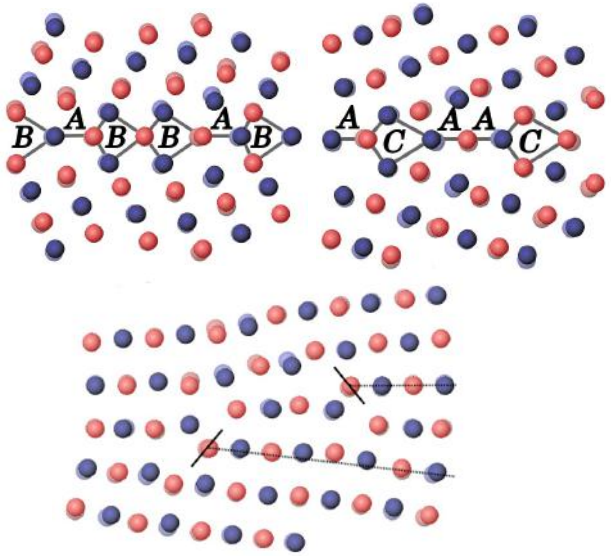

GB energy

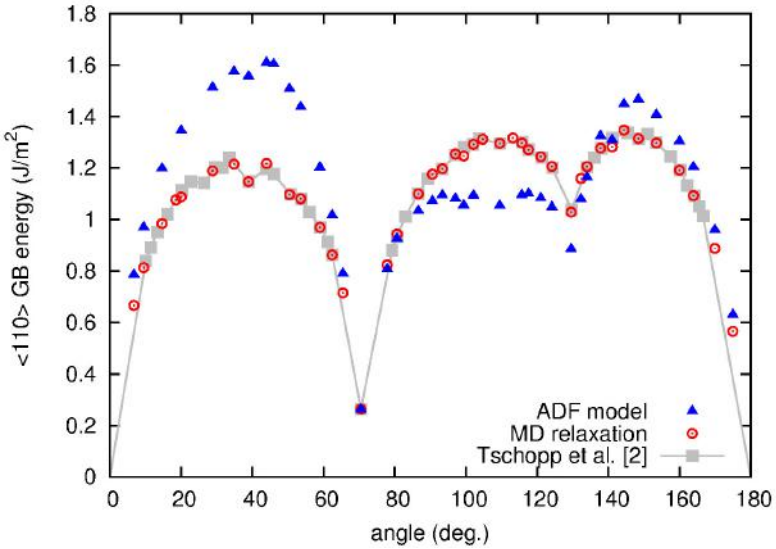

A. Kapikranyan, H. Zapolsky, C. Domain et al., Phys.Rev. B., 89, 014111, 2014.

Size-Dependent Solute Segregation at Symmetric Tilt <100> Grain Boundaries in α-Fe

Three types of solute atoms X_1, X_2 and X_3 with atomic radii $R_1 < R_{Fe}$, $R_2 = R_{Fe}$ and $R_3 > R_{Fe}$ corresponding to phosphorus (P), antimony (Sb) and tin (Sn)

Low angle GBs, with θ = 7.15 ◦ and θ = 9.53 ◦ , and two high angle GBs, Σ5 (310) (θ = 36.95 ◦) and Σ29 (730) (θ = 46.40 ◦).

Interaction potentials

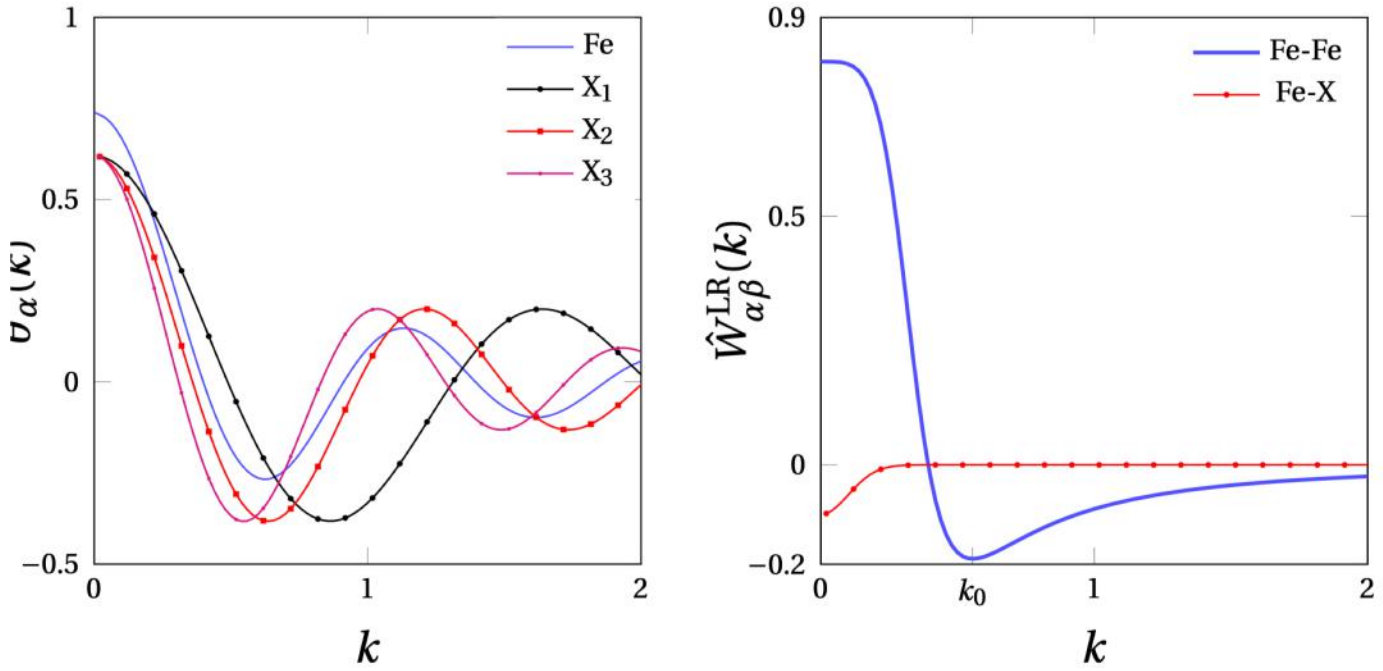

H. Zapolsky, A. Vaugeois, R. Patte, G. Demange, Materials 2021, 14, 4197.

Formation of Cottrell atmospheres around dislocations

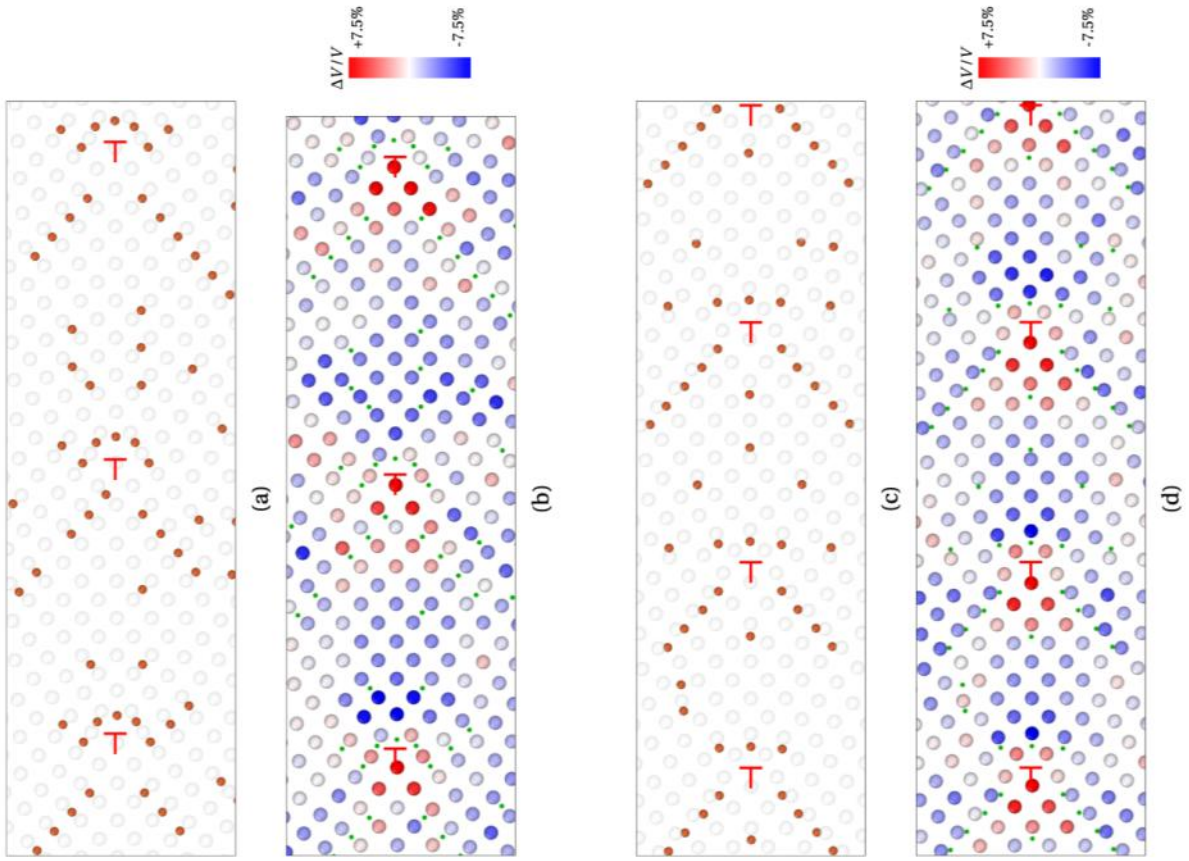

Formation of Cottrell atmospheres at ⟨100⟩ edge dislocations (red ⊢ marks) after segregation of solute atoms at ⟨100⟩ symmetric tilt LAGBs. (**a**,**b**) X_1 (small) atoms segregation for a misorientation angle $\theta = 7.15°$. (**c**,**d**) X_2 (larger) atoms for $\theta = 9.53°$. (**a**,**c**) solute atoms distribution (orange) and Fe atoms (transparent). (**b**,**d**) Volume per atom variation $\Delta V/V$ (Voronoi analysis). Red—dilatation, blue—compression. X atoms are spotted by green dots in (**b**,**d**).

HAGB in α-Fe

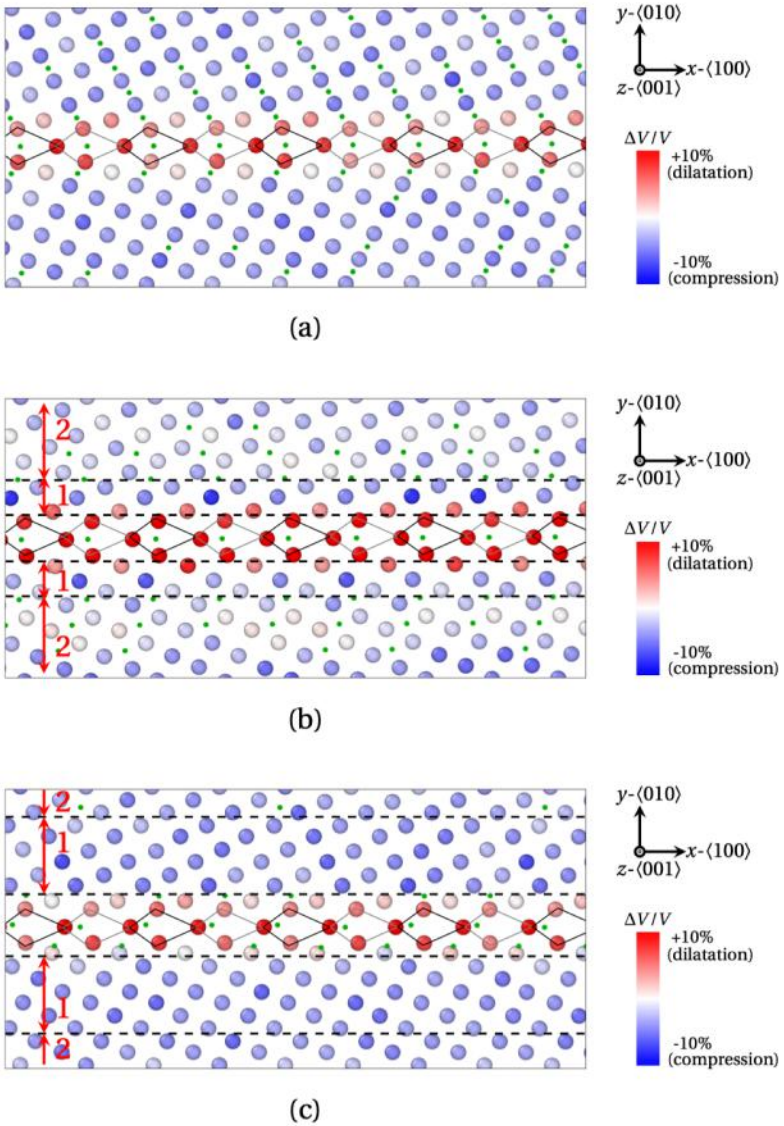

Figure 8. Influence of the volume per atom (Voronoi analysis) on th ɔn of X_1 (**a**) X_2 (**b**) and X_3 (**c**) solute atoms at Σ5 (310) ($\theta = 36.87°$). X_1 atoms are spotted by green dots. The depleted (over-compressed) and segregated (less compressed) areas are delineated by dashed black lines, and referred to as zones 1 and 2 in (**b**,**c**).

- Solute atoms are located inside of the capped trigonal prism in dilatation region.
- With increasing of atomic size the solute atoms are concentrated more and more near GB, in dilatation region

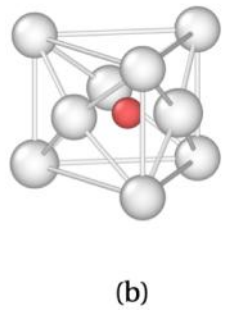

(b)

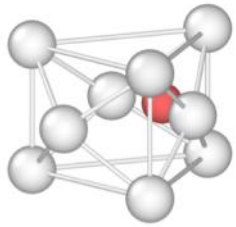

(e)

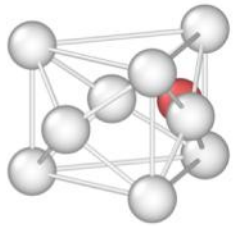

Polycrystal in α-Fe

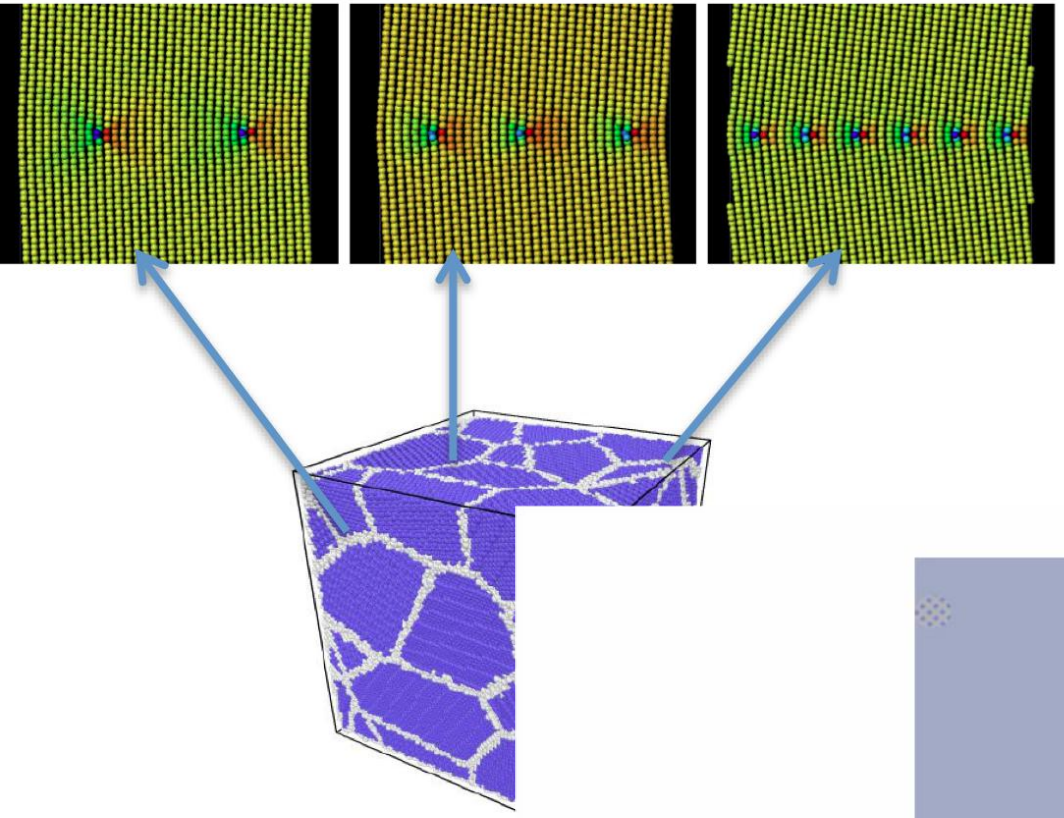

V=70^{3}nr

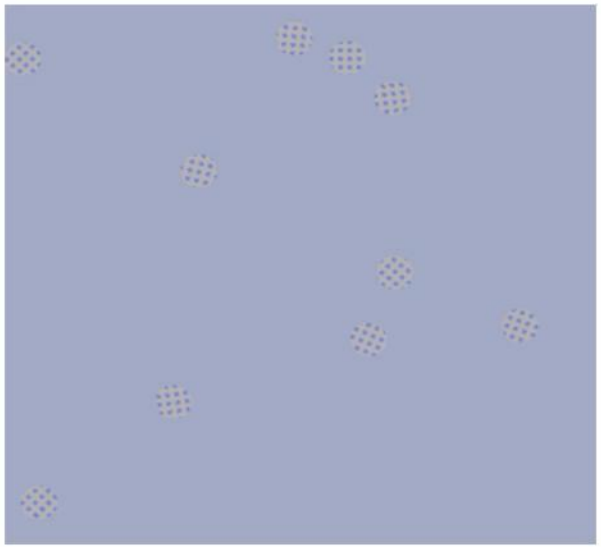

GRAIN BOUNDARIES STRUCTURE IN α-IRON UNDER APPLIED STRESS: ε=0.1

$\Sigma 5(310),\ \theta = 36.87$

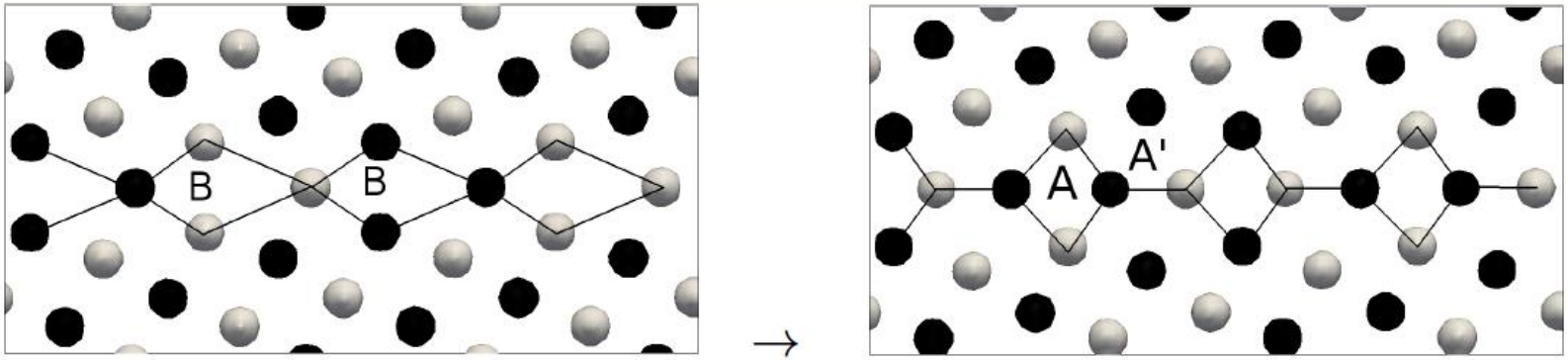

Equilibrium → Under constrain

$\Sigma 29(730),\ \theta = 46.40$

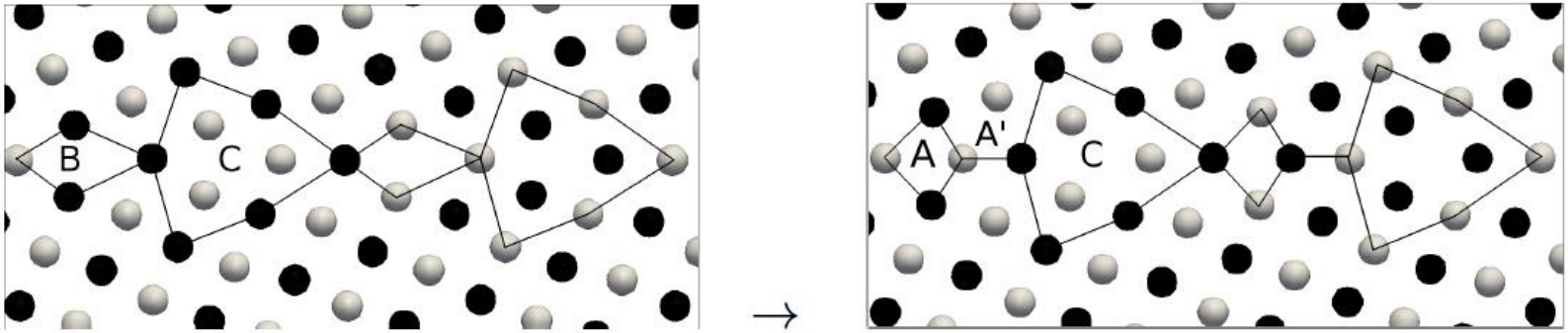

Equilibrium → Under constrain

Thesis A. Vaugeois

MARTENSITIC TRANSFORMATIONS

$$Bain\ \ OR:\ \{010\}_\gamma \| \{001\}_\alpha$$
$$\{110\}_\gamma \| \{100\}_\alpha$$

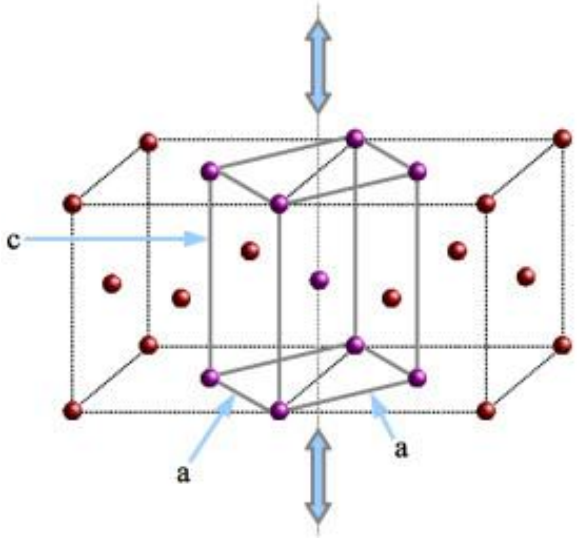

The Bain model of the martensitic transformation

$$KS\ \ OR:\ \{111\}_\gamma \| \{110\}_\alpha$$
$$\{101\}_\gamma \| \{111\}_\alpha$$

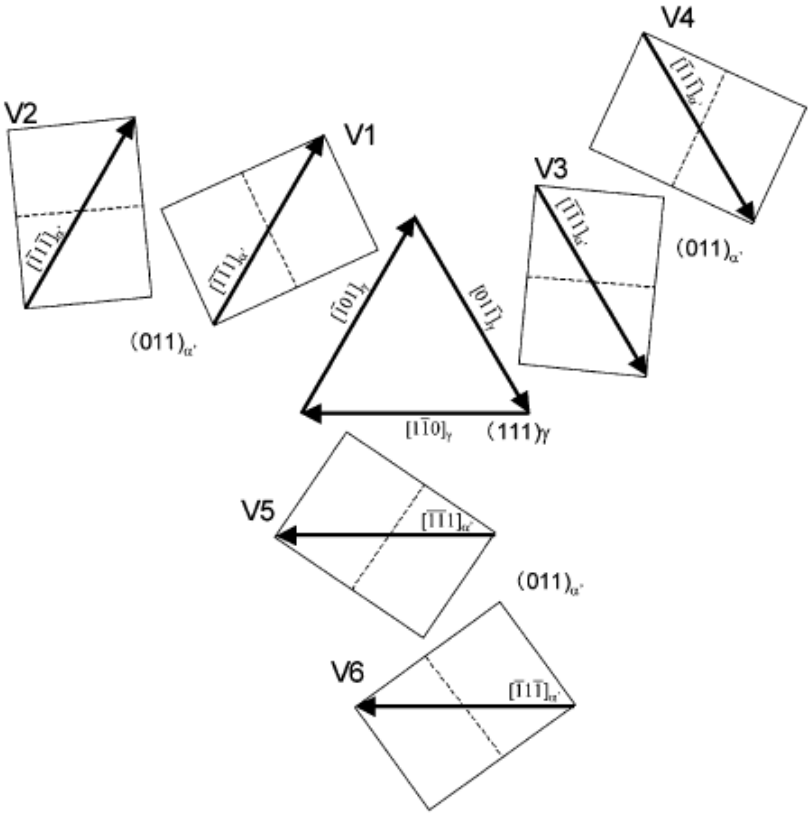

Fig. 1. Six crystallographic variants (V1–V6) for the K–S orientation relationship that evolves on a (1 1 1) austenite plane. The triangle and rectangles indicate the (1 1 1) plane of austenite (γ: fcc) and the (0 1 1) plane of martensite (α′: bcc), respectively.

MARTENSITIC TRANSFORMATIONS

The 24 crystallographic variants for the K–S orientation relationship

Variant	Plane parallel	Direction parallel
V1	$(1\,1\,1)_\gamma // (0\,1\,1)_{\alpha'}$	$[\bar{1}\,0\,1]_\gamma // [\bar{1}\,\bar{1}\,1]_{\alpha'}$
V2		$[\bar{1}\,0\,1]_\gamma // [\bar{1}\,1\,\bar{1}]_{\alpha'}$
V3		$[0\,1\,\bar{1}]_\gamma // [\bar{1}\,\bar{1}\,1]_{\alpha'}$
V4		$[0\,1\,\bar{1}]_\gamma // [\bar{1}\,1\,\bar{1}]_{\alpha'}$
V5		$[1\,\bar{1}\,0]_\gamma // [\bar{1}\,\bar{1}\,1]_{\alpha'}$
V6		$[1\,\bar{1}\,0]_\gamma // [\bar{1}\,1\,\bar{1}]_{\alpha'}$
V7	$(1\,\bar{1}\,1)_\gamma // (0\,1\,1)_{\alpha'}$	$[1\,0\,\bar{1}]_\gamma // [\bar{1}\,\bar{1}\,1]_{\alpha'}$
V8		$[1\,0\,\bar{1}]_\gamma // [\bar{1}\,1\,\bar{1}]_{\alpha'}$
V9		$[\bar{1}\,\bar{1}\,0]_\gamma // [\bar{1}\,\bar{1}\,1]_{\alpha'}$
V10		$[\bar{1}\,\bar{1}\,0]_\gamma // [\bar{1}\,1\,\bar{1}]_{\alpha'}$
V11		$[0\,1\,1]_\gamma // [\bar{1}\,\bar{1}\,1]_{\alpha'}$
V12		$[0\,1\,1]_\gamma // [\bar{1}\,1\,\bar{1}]_{\alpha'}$
V13	$(\bar{1}\,1\,1)_\gamma // (0\,1\,1)_{\alpha'}$	$[0\,\bar{1}\,1]_\gamma // [\bar{1}\,\bar{1}\,1]_{\alpha'}$
V14		$[0\,\bar{1}\,1]_\gamma // [\bar{1}\,1\,\bar{1}]_{\alpha'}$
V15		$[\bar{1}\,0\,\bar{1}]_\gamma // [\bar{1}\,\bar{1}\,1]_{\alpha'}$
V16		$[\bar{1}\,0\,\bar{1}]_\gamma // [\bar{1}\,1\,\bar{1}]_{\alpha'}$
V17		$[1\,1\,0]_\gamma // [\bar{1}\,\bar{1}\,1]_{\alpha'}$
V18		$[1\,1\,0]_\gamma // [\bar{1}\,1\,\bar{1}]_{\alpha'}$
V19	$(1\,1\,\bar{1})_\gamma // (0\,1\,1)_{\alpha'}$	$[\bar{1}\,1\,0]_\gamma // [\bar{1}\,\bar{1}\,1]_{\alpha'}$
V20		$[\bar{1}\,1\,0]_\gamma // [\bar{1}\,1\,\bar{1}]_{\alpha'}$
V21		$[0\,\bar{1}\,\bar{1}]_\gamma // [\bar{1}\,\bar{1}\,1]_{\alpha'}$
V22		$[0\,\bar{1}\,\bar{1}]_\gamma // [\bar{1}\,1\,\bar{1}]_{\alpha'}$
V23		$[1\,0\,1]_\gamma // [\bar{1}\,\bar{1}\,1]_{\alpha'}$
V24		$[1\,0\,1]_\gamma // [\bar{1}\,1\,\bar{1}]_{\alpha'}$

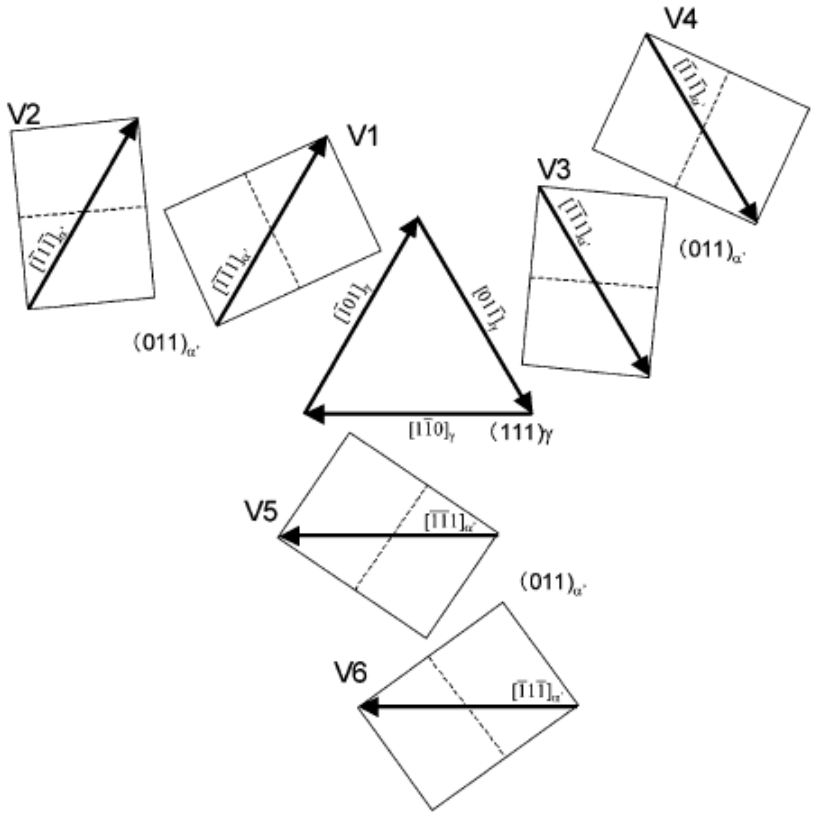

Fig. 1. Six crystallographic variants (V1–V6) for the K–S orientation relationship that evolves on a (1 1 1) austenite plane. The triangle and rectangles indicate the (1 1 1) plane of austenite (γ: fcc) and the (0 1 1) plane of martensite (α′: bcc), respectively.

FCC-BCC transition

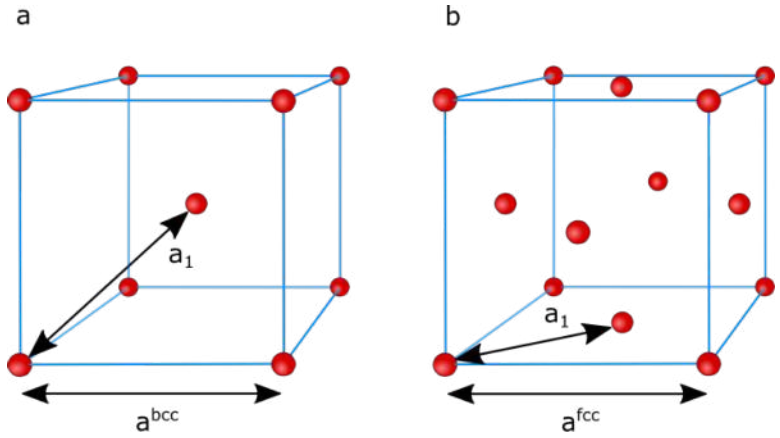

$$\frac{a_0^{fcc}}{a_0^{bcc}} = \sqrt{\frac{3}{2}} \approx 1.225 \qquad a_0^{fcc} = 8\Delta x$$

$$\sigma = 0.05$$

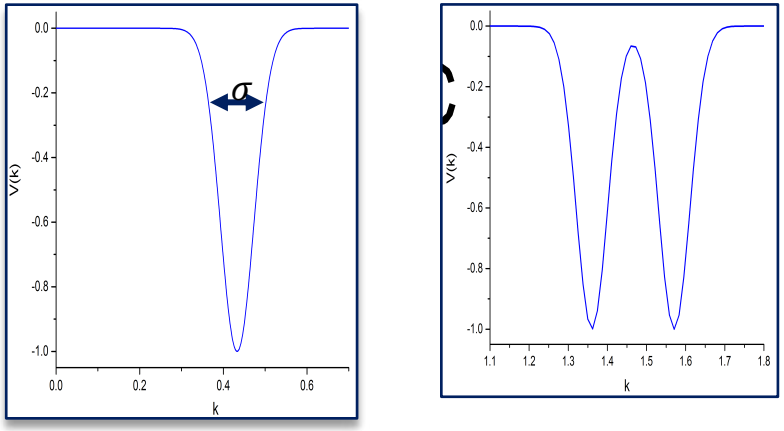

Elastic constants of the given potential

$$\frac{C_{11}^{bcc}}{C_{11}^{fcc}} \approx 1.68, \quad \frac{C_{12}^{bcc}}{C_{12}^{fcc}} \approx 1.25, \quad \frac{C_{44}^{bcc}}{C_{44}^{fcc}} \approx 1.3$$

Experimental elastic constants for iron

$$\frac{C_{11}^{bcc}}{C_{11}^{fcc}} \approx 1.60, \quad \frac{C_{12}^{bcc}}{C_{12}^{fcc}} \approx 1.15, \quad \frac{C_{44}^{bcc}}{C_{44}^{fcc}} \approx 1.51$$

$$\tilde{w}_{LR}(\mathbf{k}) = \exp\left(-\frac{(k-k_{01})^2}{2\sigma^2}\right) + 0.1\exp\left(-\frac{(k-k_{02})^2}{2\sigma^2}\right)$$

Twinning structure of α-Fe (bcc) precipitate in Cu (fcc) matrix in the Cu-2.0Fe-0.5Co wt%

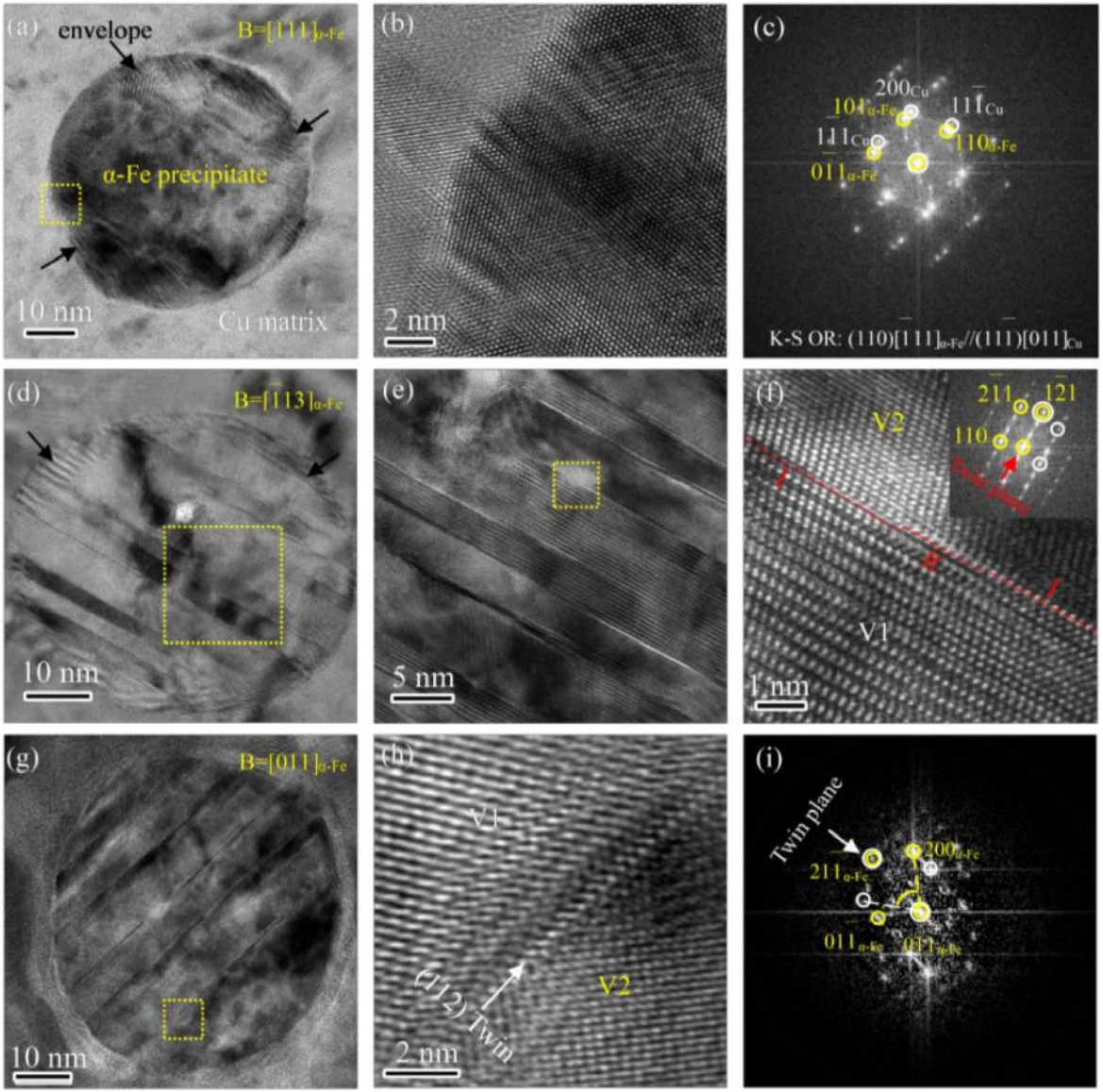

Growth of α-Fe particle in the Cu matrix

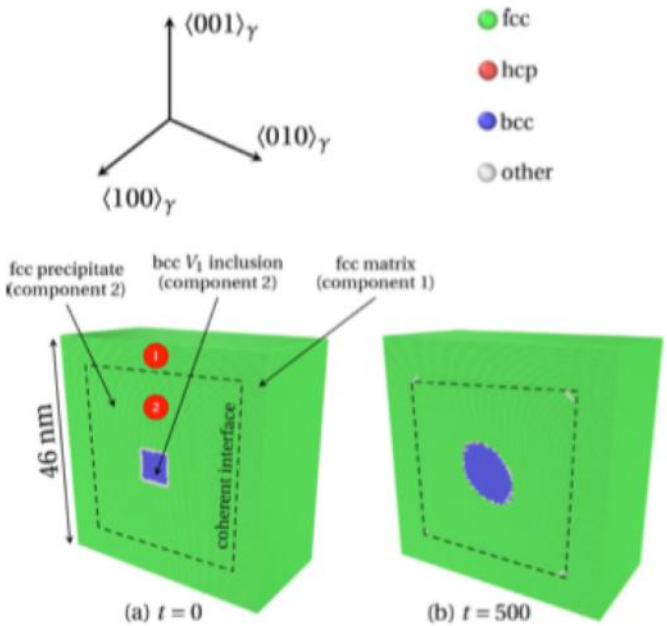

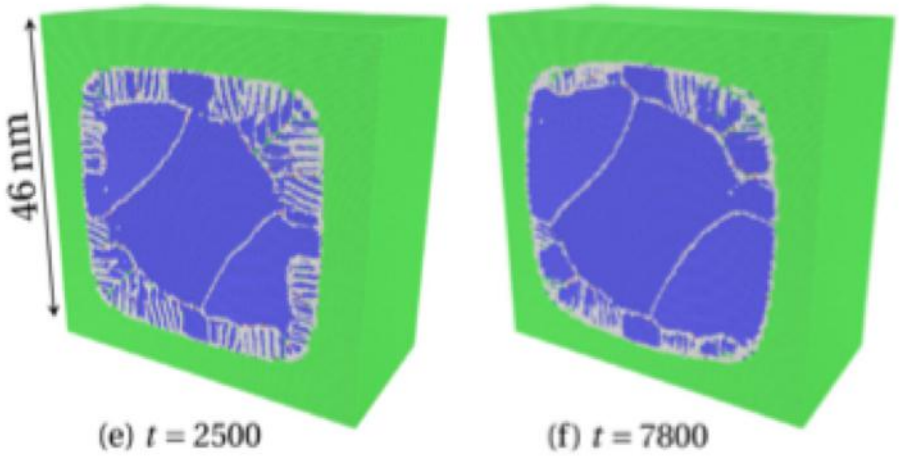

Two-variants structure with Kurdjumov–Sachs OR

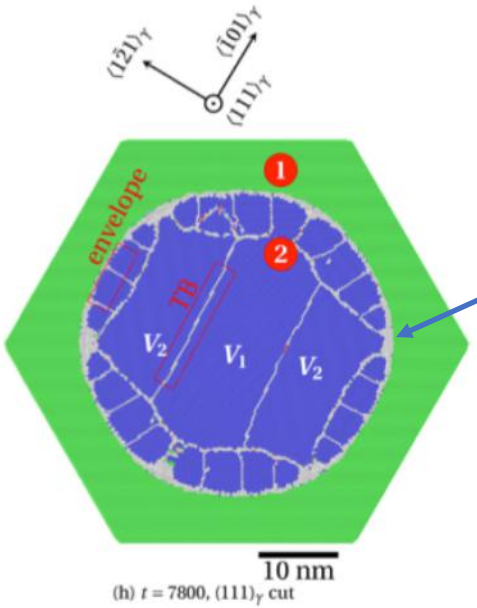

Size of the simulation box 1024^3
46^3 nm

G. Demange et al. Acta mat. 226 (2022)

Twin boundaries

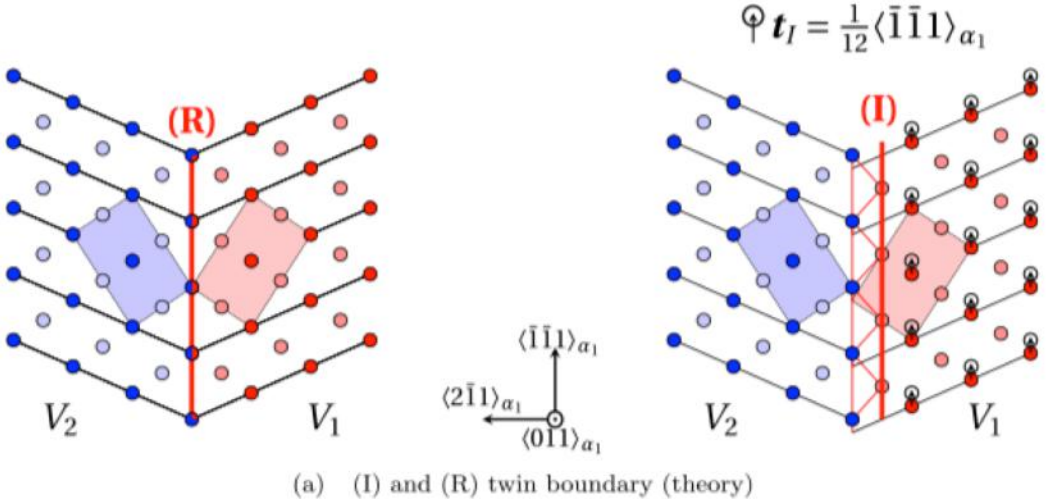

(a) (I) and (R) twin boundary (theory)

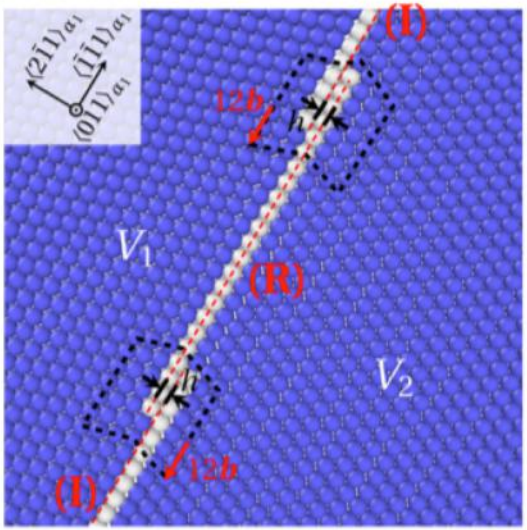

(a) IR+RI couple

Reflection (R) and isoceles(I) twin boundaries structures

During the propagation of TB, the transitions (I) → (R) and (R) → (I)– is accompanied by the stacking fault in $(\bar{2}11)_{\alpha 1}$ planes, which results in the shift of the interface along the direction $\langle \bar{2}11 \rangle_{\alpha 1}$ perpendicular to the twinning plane.

Partial twin dislocation couple (IR+RI) with step

h = $a_2(2\sqrt{6})$, Burgers vector **b** = $\frac{1}{12} < \bar{1}11 >_{\alpha 1}$

Fcc/bcc interface

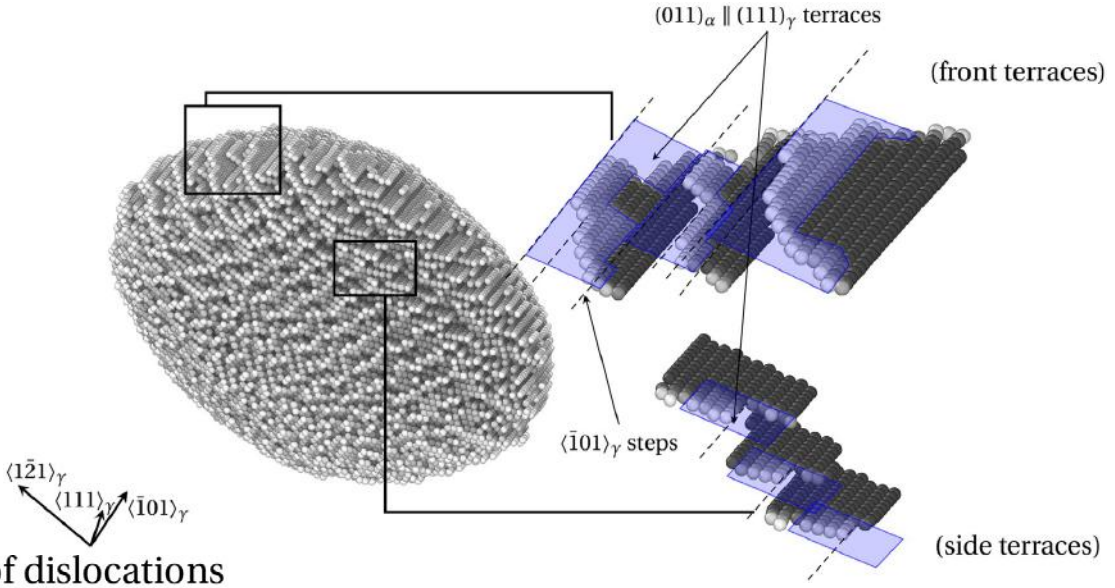

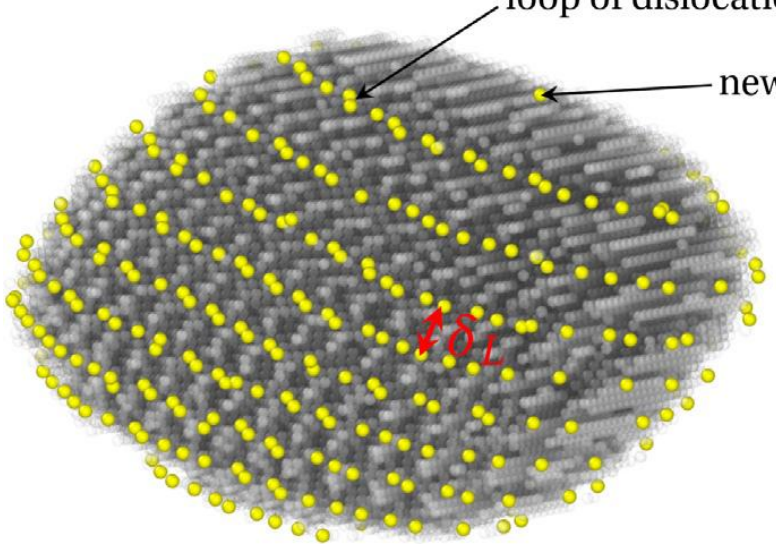

3D distribution of screw dislocation cores (yellow spheres). fcc screw dislocations $\mathbf{b_2} = \pm 1/2\langle 110 \rangle_\gamma$

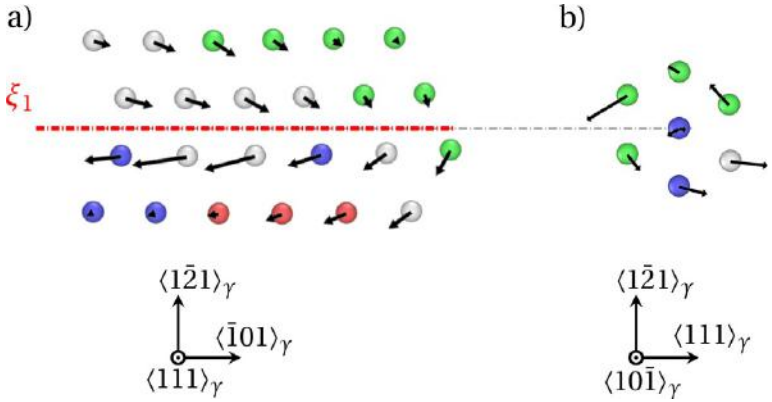

Propagation mechanism of fcc/bcc interface

Screw dislocations:

$\mathbf{b_1} = \pm 1/2\langle \bar{1}01 \rangle_\gamma$

$\mathbf{b_2} = \pm 1/2\langle 1\bar{1}0 \rangle_\gamma$

Partial Shockley

$b_p = \pm 1/6\langle 1\bar{2}1 \rangle_\gamma$

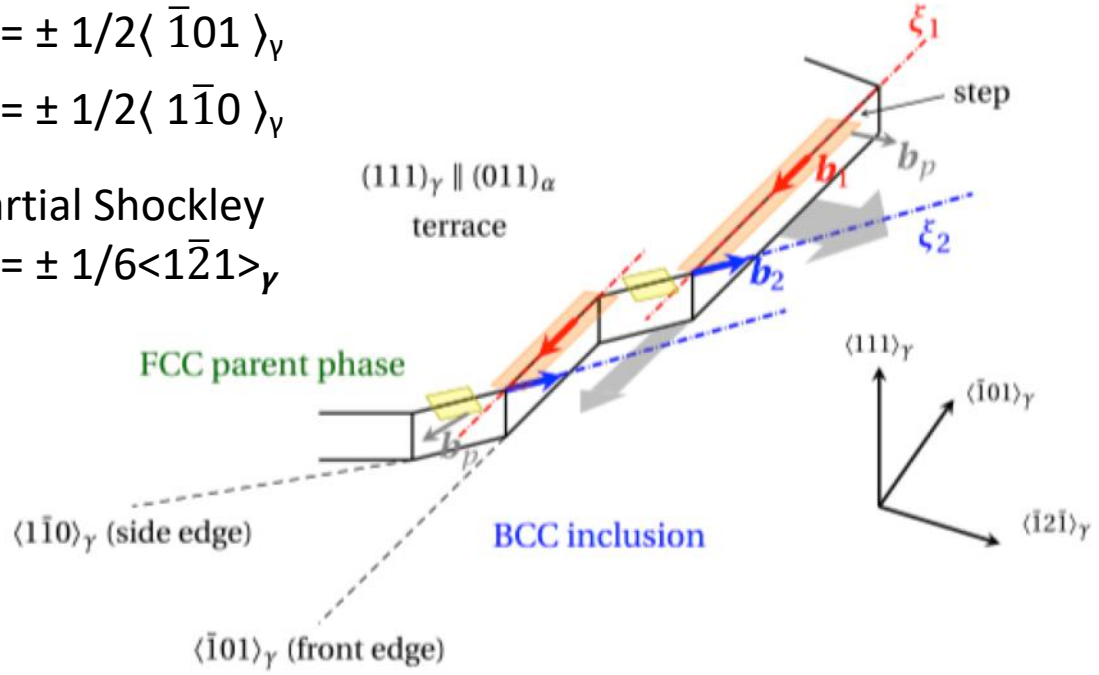

Transformation pass: fcc → hcp → bcc.

Two steps:

- Shockley partial dislocation with Burgers vector $\mathbf{b}_p$ produces a SF ABCABC-> ABAB
- Homogeneous deformation $(111)_\gamma$ fcc -> $(011)_\alpha$ bcc planes (glide of $\mathbf{b}_1$ and $\mathbf{b}_2$ fcc screw dislocations)

Dual-phase (DP) steels

Dual microstructure of soft ferrite and harder martensite phases.

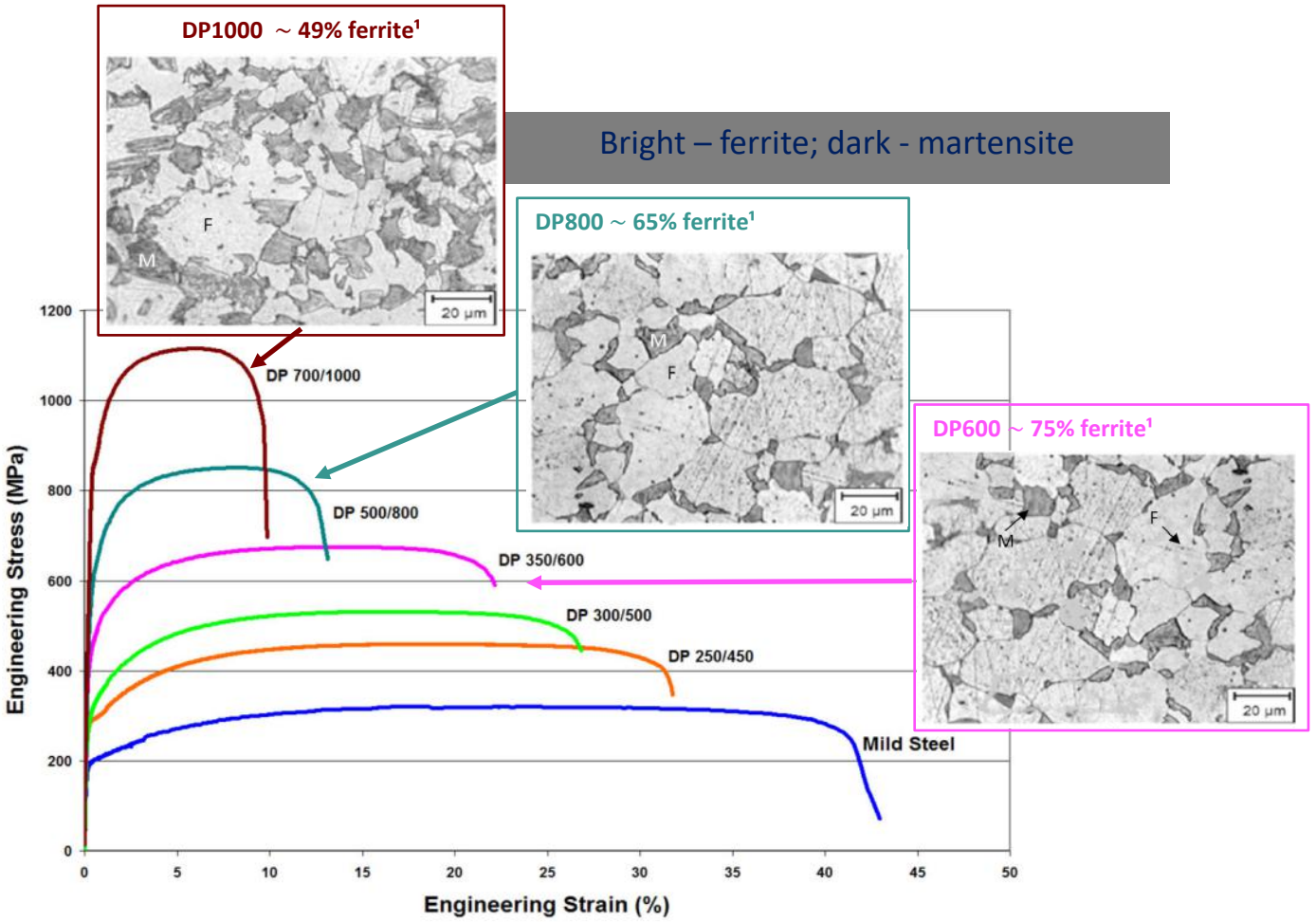

Role of transformation interface

Solid-state phase transformations during steel processing

Microstructure future

- phases volume fraction
- topology and morphology of phases
- grain size distribution

Mechanical properties of the steel

moving transformation interface

???

- Interface interaction with the alloying elements
- Orientation relationship (ORs) between two phases
- Interface properties (coherency, thickness and shape)
- Atomic structure of the interface
- Ability to dissipate energy: interfacial friction

Experimental investigation of the transformation interface at the nanoscale and **modeling**

15s at 625 °C: interface #7

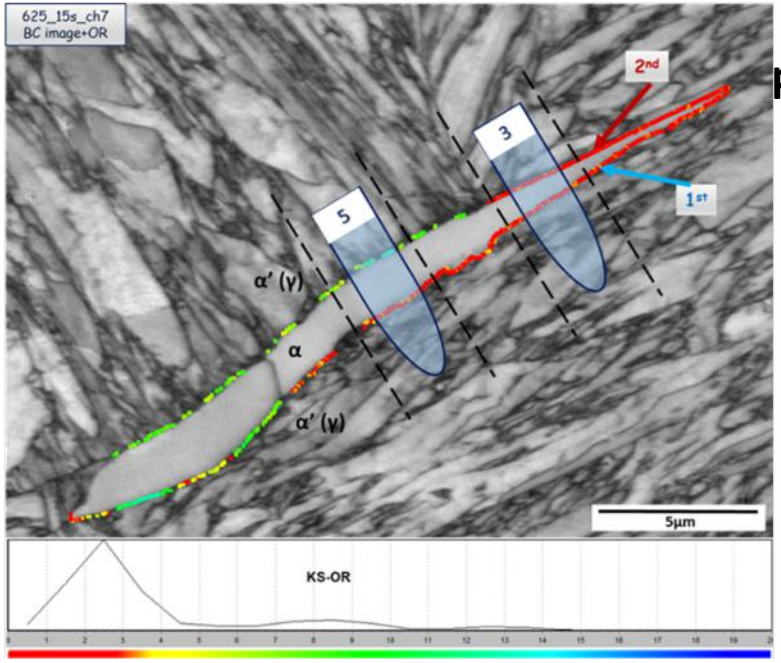

p 4

tip3_2nd

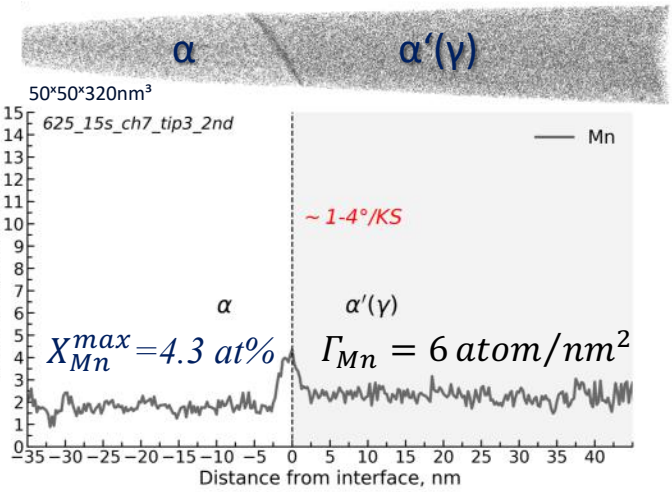

tip5_2nd

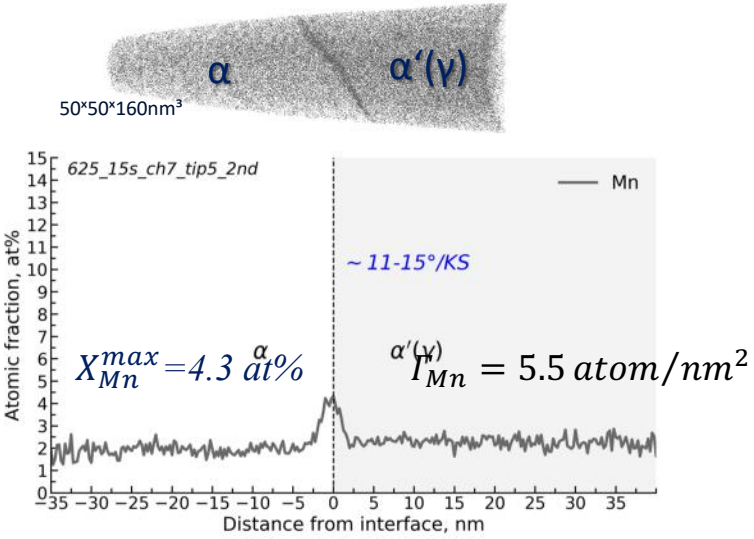

Thesis O. Nakonechna

Austenite-to-ferrite phase transfromation

- The change in the crystal structure (from fcc to bcc).
- Diffusional process: the redistribution of interstitial and substitutional elements.

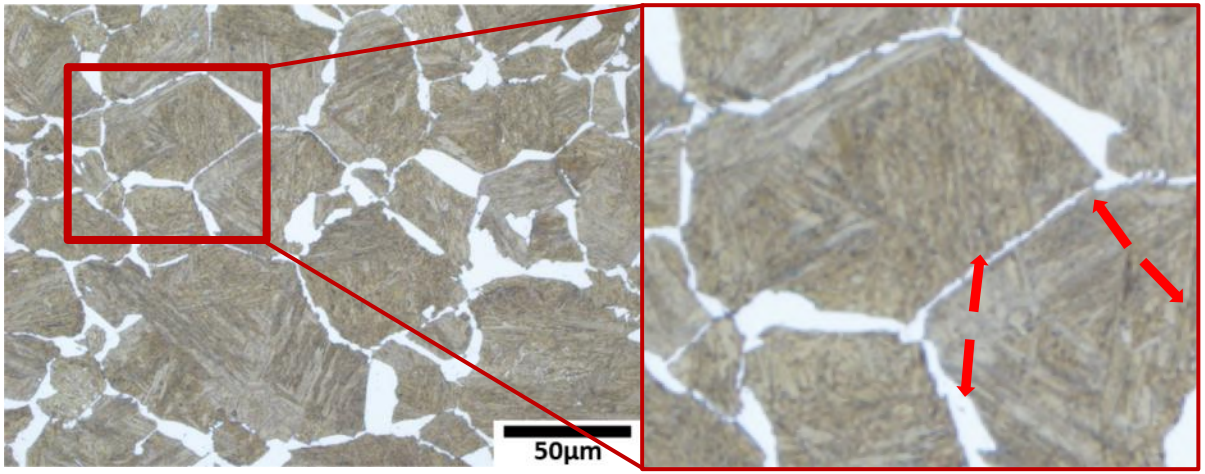

Kurdjumov-Sachs (KS):

$\{111\}_\gamma$ II $\{110\}_\alpha$

$\langle\bar{1}01\rangle_\gamma$ II$\langle\bar{1}\bar{1}1\rangle_\alpha$

Nishiyama-Wassermann (NW):

$\{111\}_\gamma$ *II* $\{011\}_\alpha$

$\langle 10\bar{1}\rangle_\gamma$ *II*$\langle 100\rangle_\alpha$

At higher T: disordered interfaces migrate faster
At lower T: coherent interfaces migrate faster [1]

FCC-BCC plane interface

Greninger-Troiano OR

Kurdjumov-Sachs OR

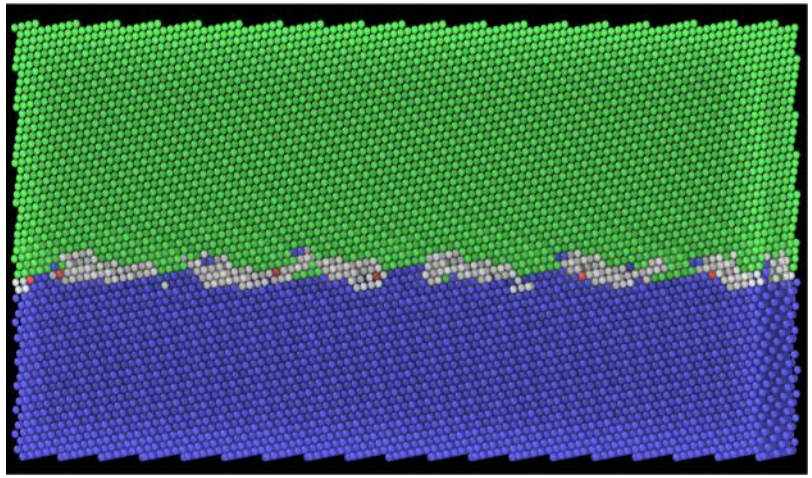

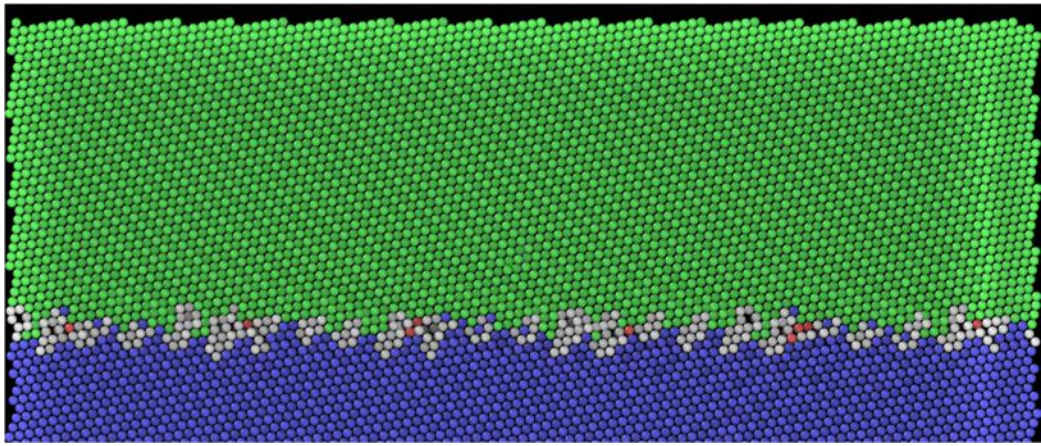

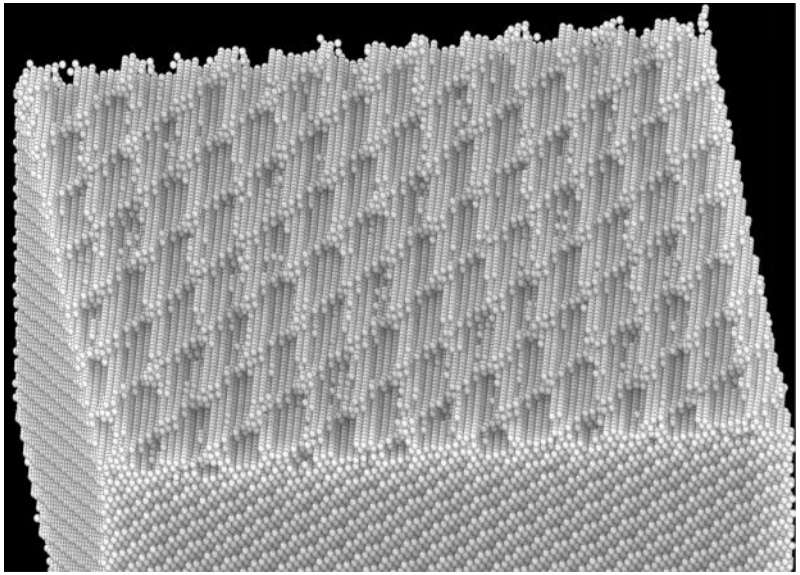

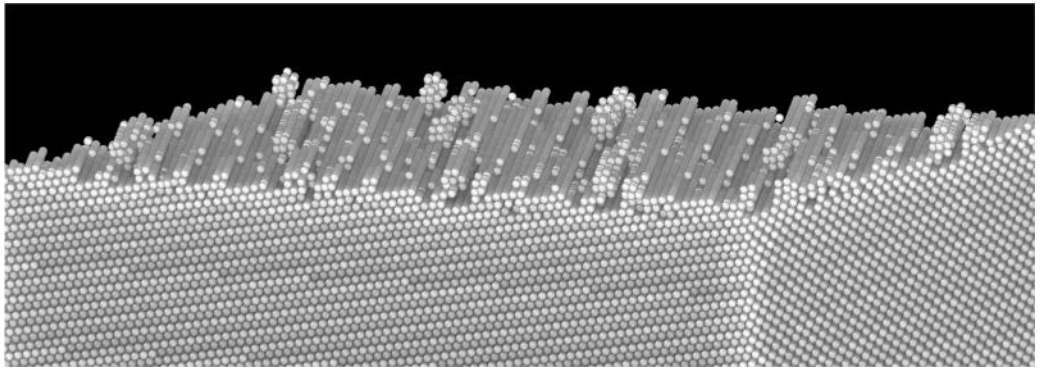

Thesis Y. Borges Gomes Lima

Propagation of (575) interface with KS OR

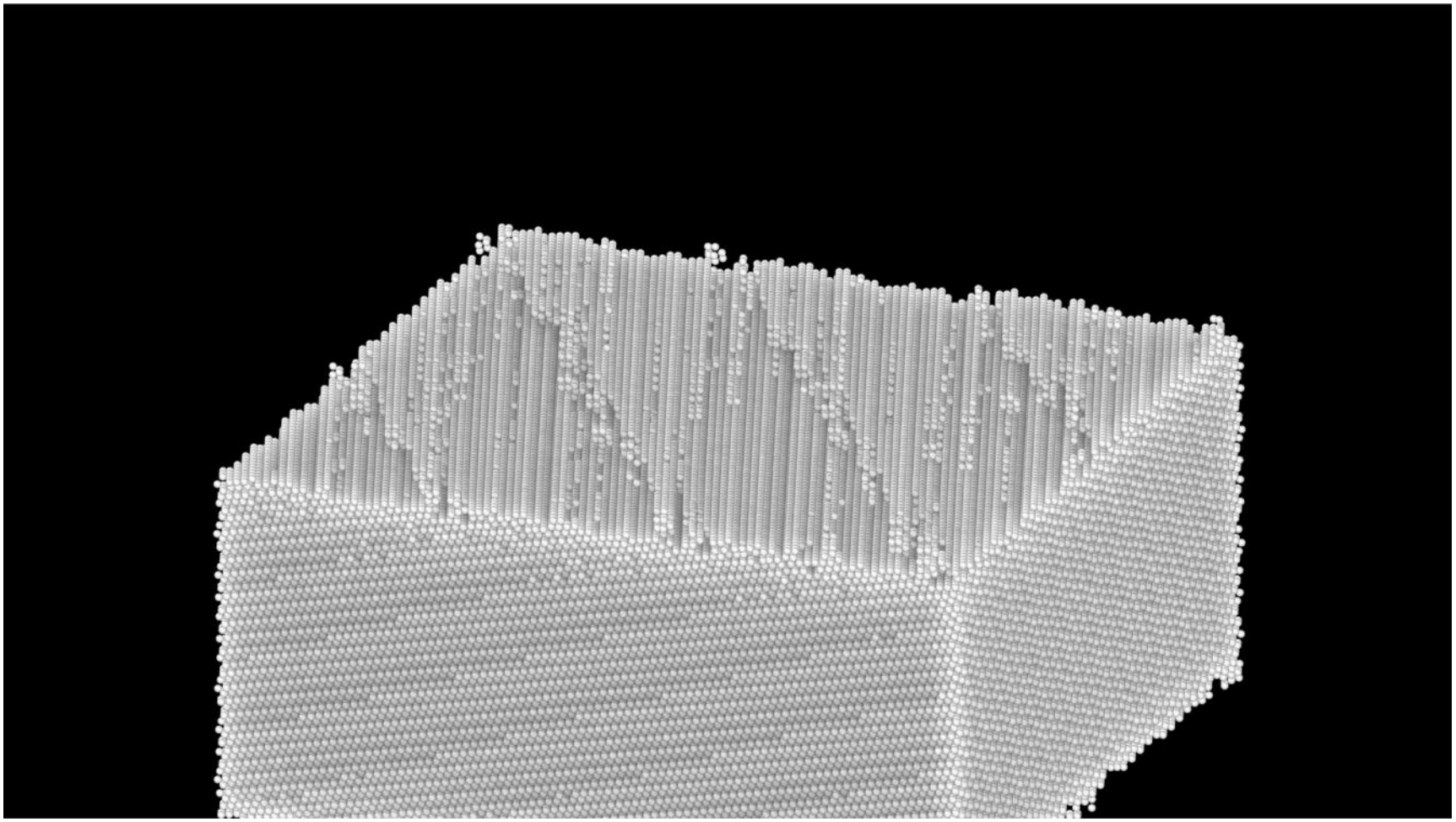

Nishiyama Wasserman Orientation Relationship

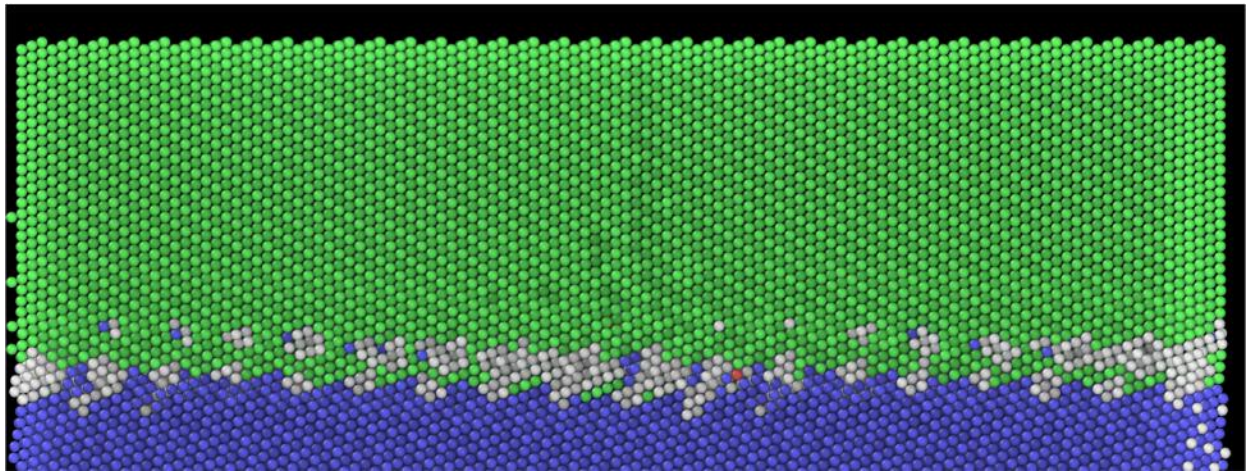

(121) Habit plane

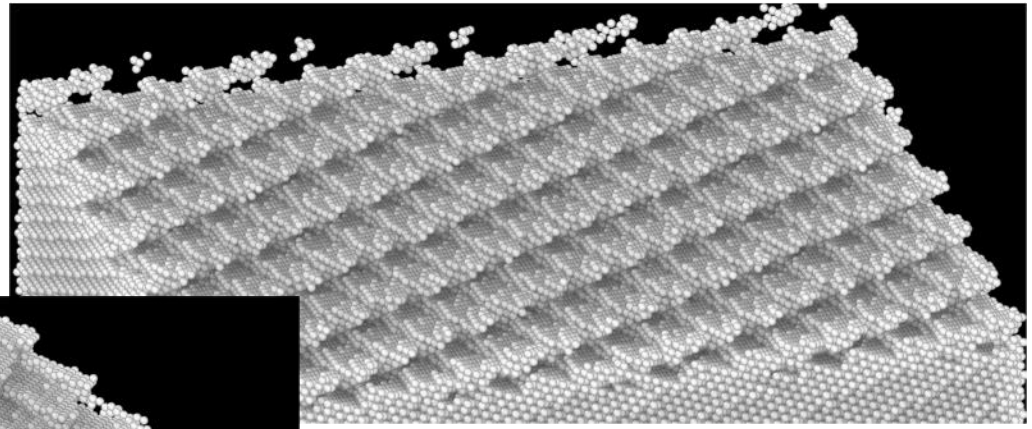

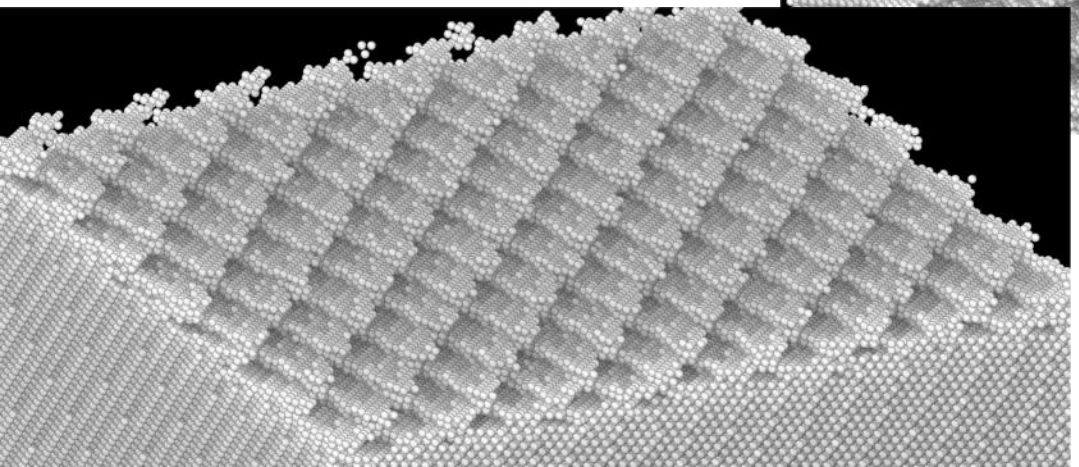

(575) Habit plane

FCC->BCC phase transformation in Fe

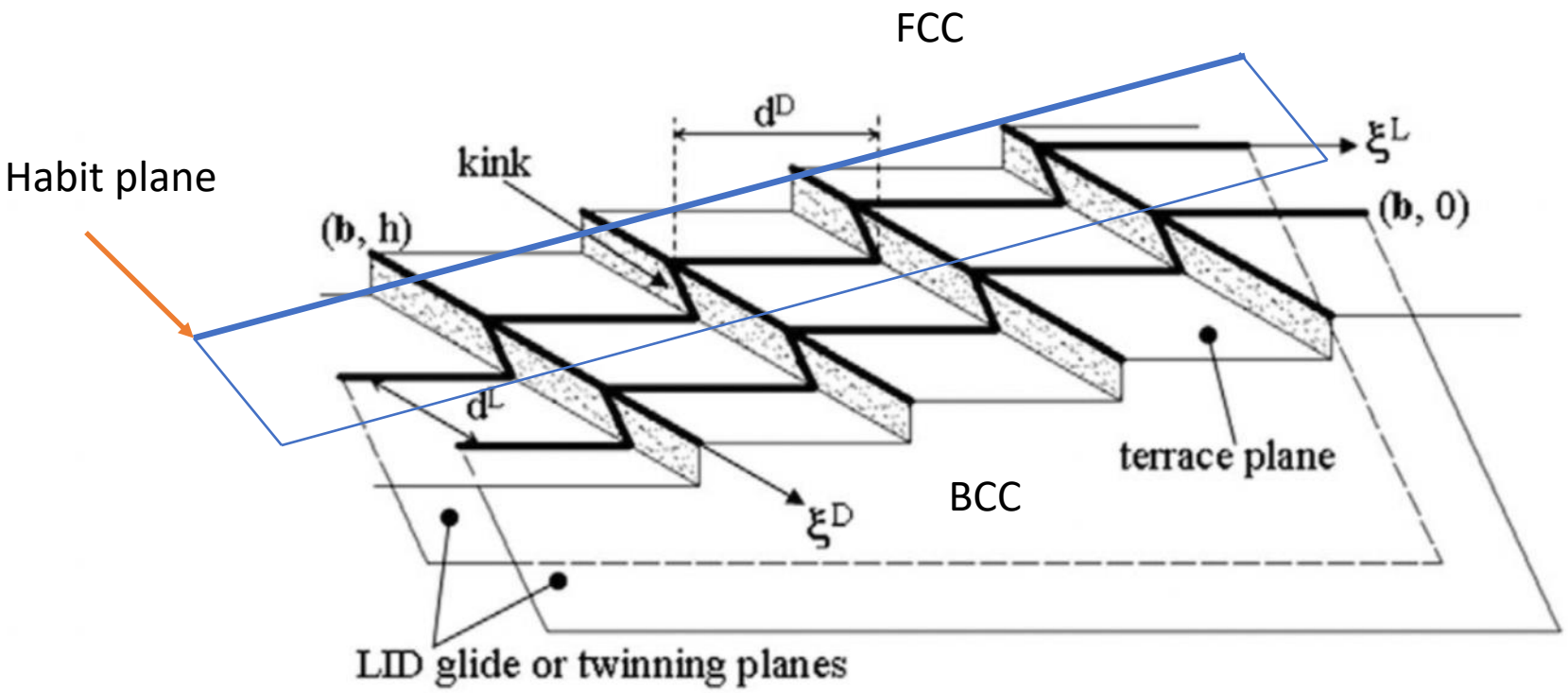

To identify the crystal defects

↓

Slip Vector Analysis (SVA)

Nishiyama Wasserman Orientation Relationship

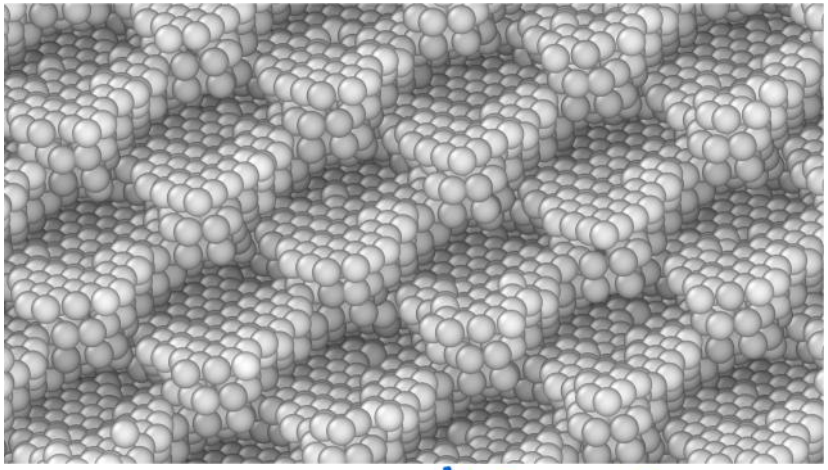

- Average step height : $h = a_{BCC}\sqrt{3} \approx 0{,}50\ \text{nm}$.
- Average terrace length : $1{,}0\ \text{nm} \leq l \leq 1{,}5\text{nm}$.

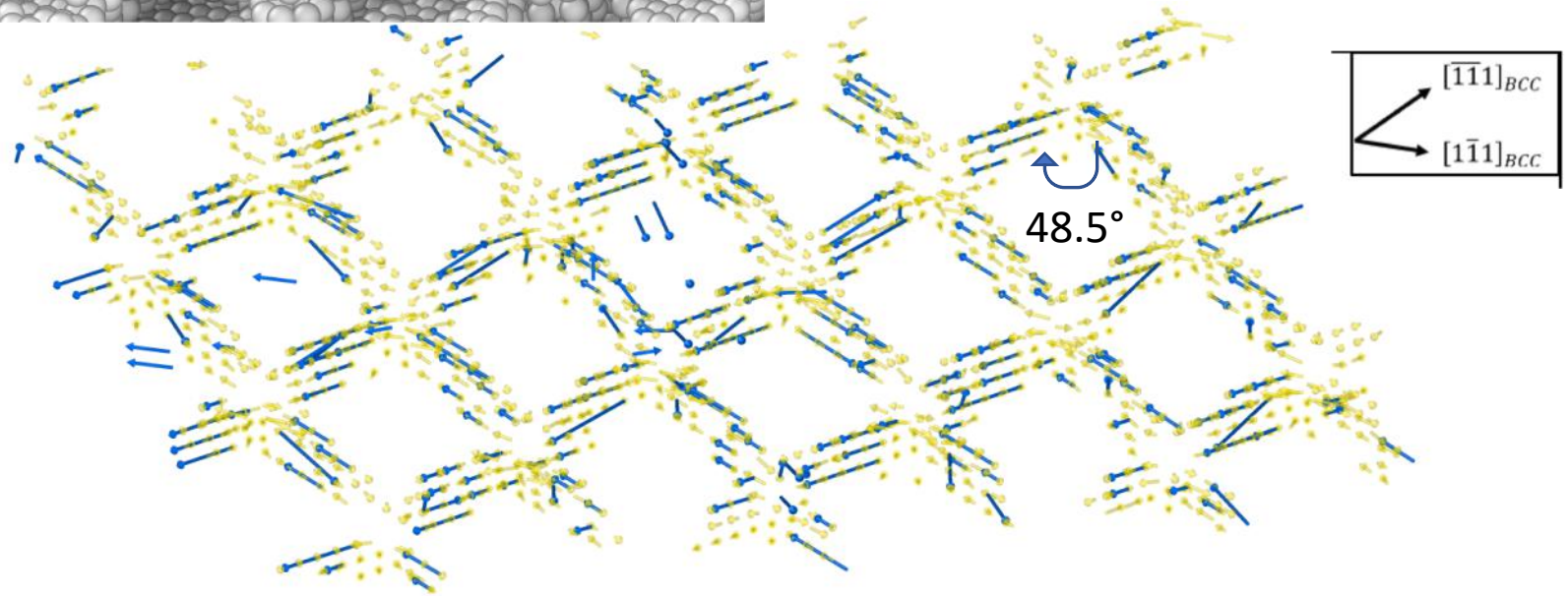

Slip Vector Aanalyses of NW $(575)_{FCC}$ interface with a BCC reference. Blue vectors are detected dislocations mean line direction.

Kurdjumov-Sachs OR

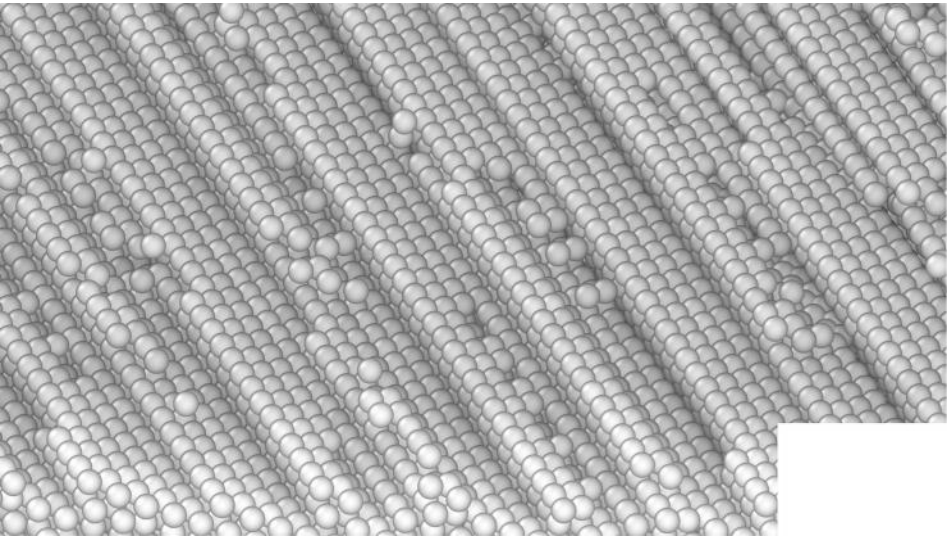

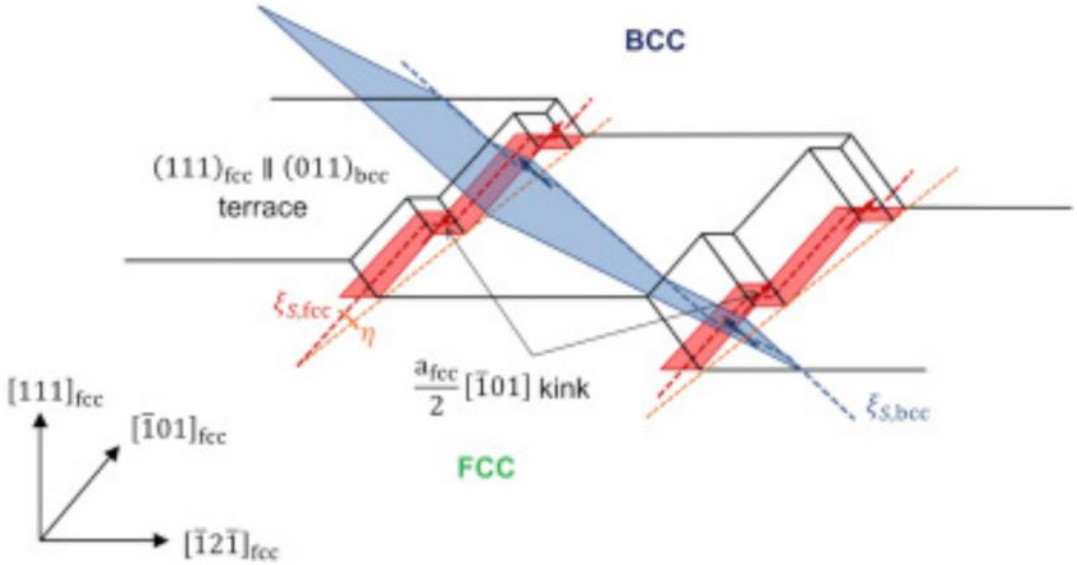

screw dislocations exist with Burgers vector $a_{fcc}/2[\bar{1}01]$ lying next to the steps along $[101]_{fcc}$, with the stacking fault between partials lying on the $(111)_{fcc}$ terrace.

F. Maresca et W. A. Curtin, Acta Mat., 134, 2017

Interaction of the Fcc/BCC interface with Carbon atoms

Long-range potential to model the C-C repulsion:

$$w_{CC}^{LR}(\boldsymbol{r}) = \begin{cases} 0, & if\ r < (R_C + \Delta R_C) \\ e^{-\alpha r}, & if\ r \geq (R_C + \Delta R_C) \end{cases}$$

$$\alpha = 0.34 \ [2]$$

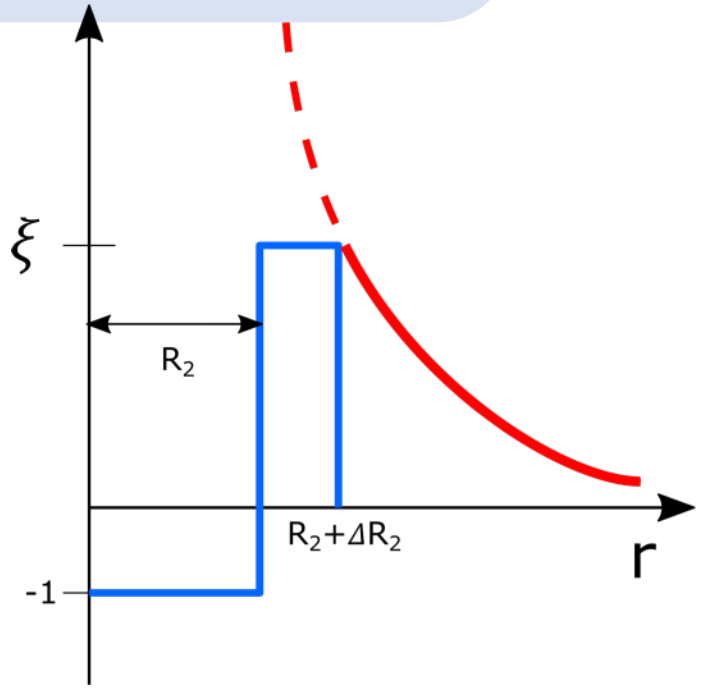

[2] *A.Udyansky, J. von Pezold, A.Dick, and J.Neugebauer, Phys. Rev. B **83**, 184112, 2011*

Long-range potential to model the Fe-C repulsion (Screened Coulomb potential):

$$w_{FeC}(\boldsymbol{r}) = \frac{e^2}{r}\exp\left(-\frac{\boldsymbol{r^2}}{r_D^2}\right)$$

$r_D = 0.2036 \cdot a_0$ [3], where r_D - *Debye radius*

$$w_{FeC}(\boldsymbol{k}) = \lambda_2 \frac{1}{(1/r_D)^2 + k^2}$$

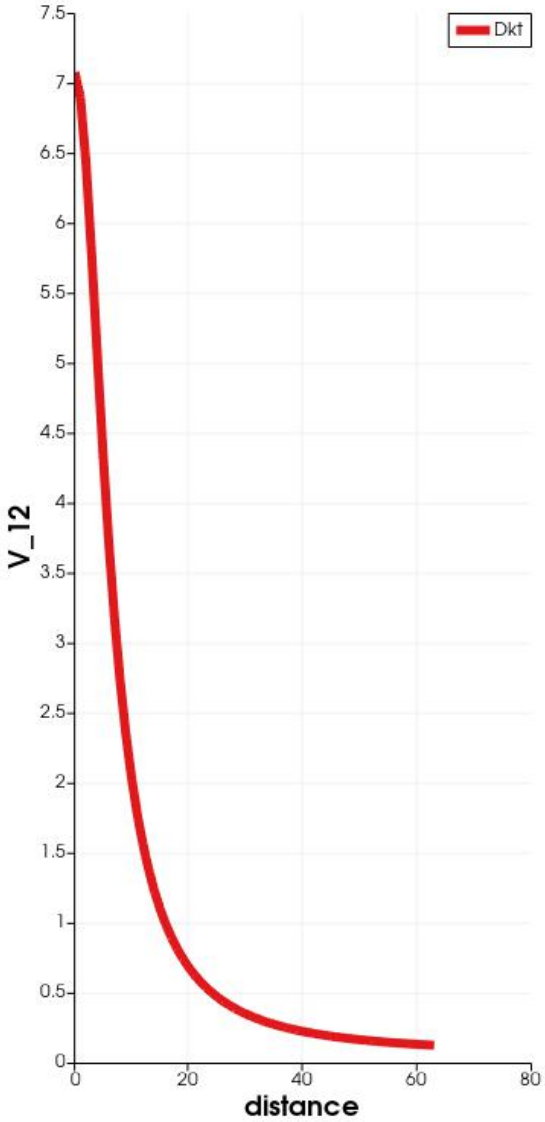

[3] *Khachaturyan, Pokrovskii, Progress in Materials Science Vol. 29, pp. 1-138, 1985*

$$\hat{L}^0 = \begin{pmatrix} L^0_{FeFe} & L^0_{FeC} \\ L^0_{FeC} & L^0_{CC} \end{pmatrix}$$

- $L^0_{FeC} = 0$ - since C atoms are in interstitial positions, there is no Fe/C exchange

- $L^0_{CC}/L^0_{FeFe} > 1$ – Carbon atoms are more mobile than iron atoms

$$\hat{L}^0 = \begin{pmatrix} 0.67 & 0 \\ 0 & 1.5 \end{pmatrix}$$

Segregation of C atoms at non-KS interfaces

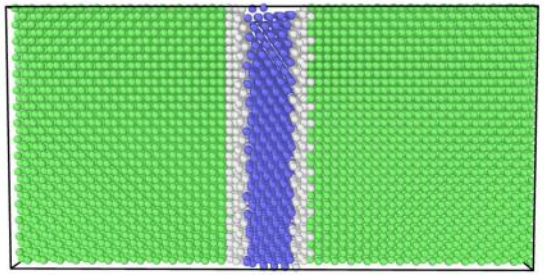

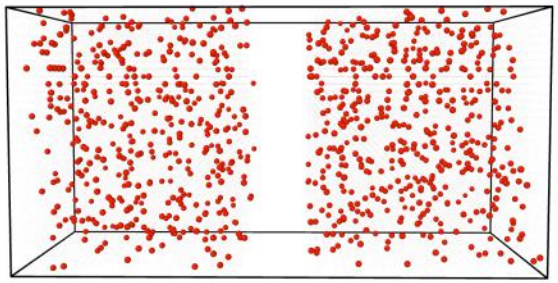

OVITO software: Common Neighbor Analysis (CAN)

- **BCC;**
- **FCC;**
- **“other”;**
- **Carbon**

$V = 256 \times 256 \times 512$

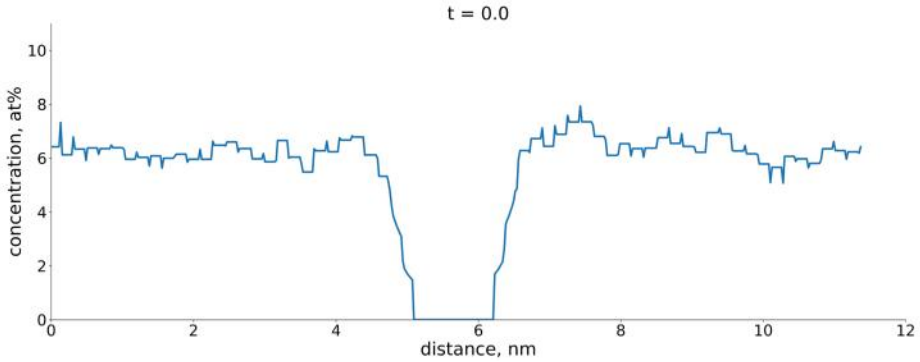

Segregation of C atoms at non-KS interfaces

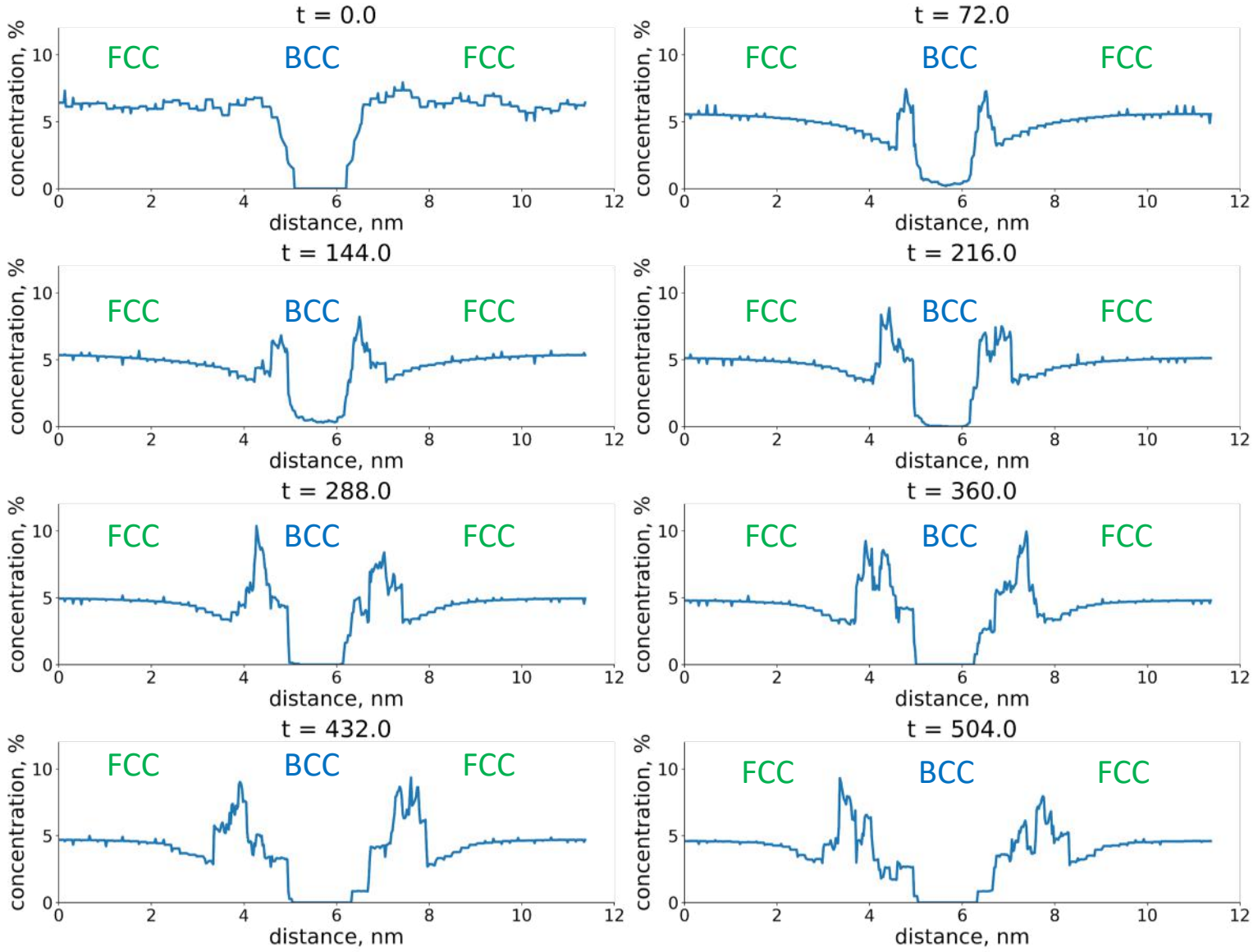

APT data Fe-0,787At%C-2At%Mn

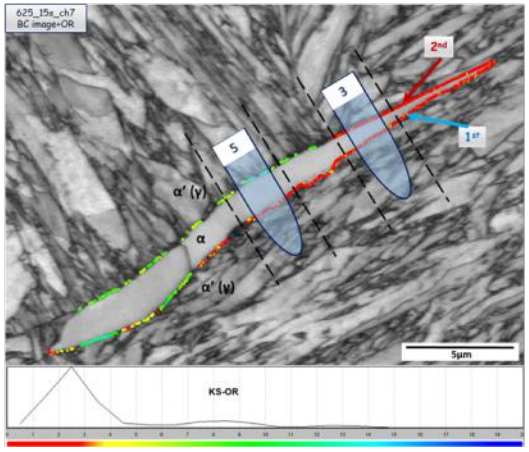

(a)

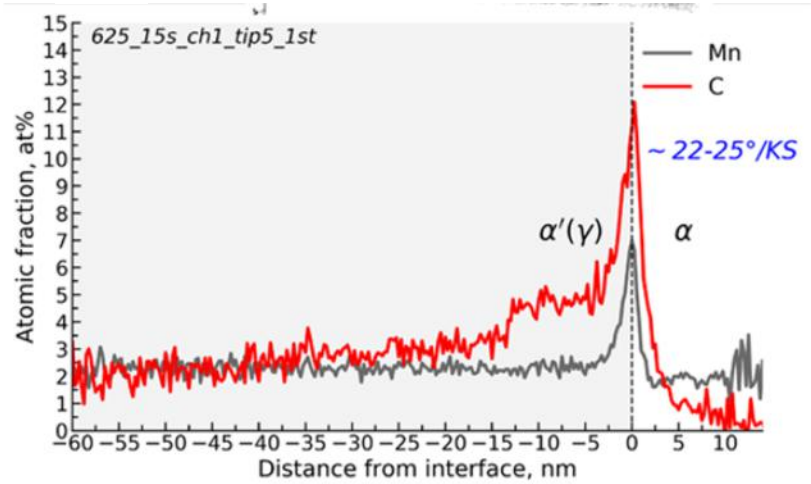

(b)

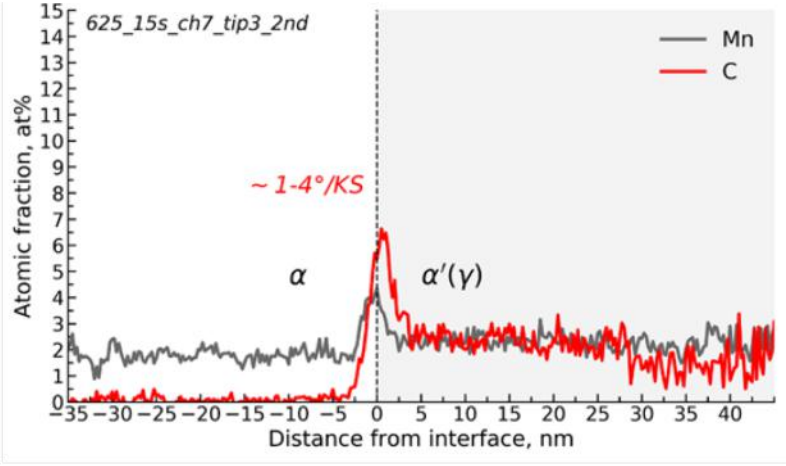

3D reconstructions and concentration profiles of C and Mn atoms across (**a**) the 1st interface of tip5 (isothermal holding at 625°C during 15s),

(**b**) the 2nd interface of tip3 (isothermal holding at 625°C during 15s).

Thesis O. Nakonechna

Segregation of C atoms at fcc/bcc moving interface

FCC/BCC interface with C atoms

- Interface with Non-KS OR propagates faster than KS
- Concentration of C at non-KS OR interface is around 12%
- Concentration of C at KS OR interface is around 5-6 %

Versatility of Phase Field Atomic and Nanoscale Modeling

$$\frac{\partial c(\mathbf{r},t)}{\partial t} = \left(\nabla M \nabla\right)\frac{\delta F}{\delta c}$$

$$\frac{\partial \eta(\mathbf{r},t)}{\partial t} = -L\frac{\delta F}{\delta \eta}$$

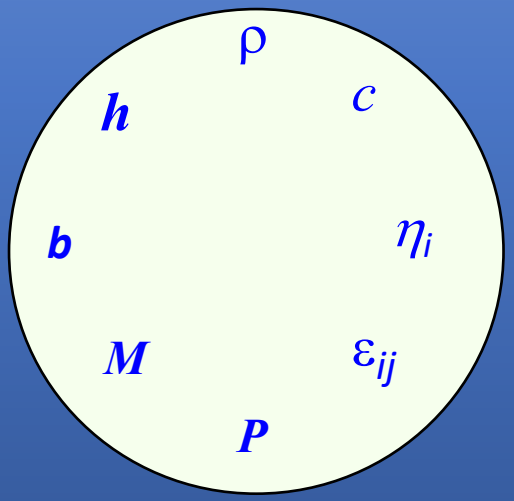

Different types of fields:

- atomic density, $\rho(r)$ –solidification, atomic ordering
- composition $c(r)$, decomposition
- atomic LRO parameters, $\eta(r)_i$, (atomic ordering)
- transformation strain, $\varepsilon(r)_{ij}$, (martensitic transformation)
- polarization, P, (ferroelectrics)
- magnetization, $M(r)$, (ferromagnets)
- Burgers vector, b, (multi-dislocations systems)
- crack opening, h (multi-crack systems)